INFORMATION TO USERS

This manuscript has been reproduced from the microfilm master. UMI films the text directly from the original or copy submitted. Thus, some thesis and dissertation copies are in typewriter face, while others may be from any type of computer printer.

The quality of this reproduction is dependent upon the quality of the copy submitted. Broken or indistinct print, colored or poor quality illustrations and photographs, print bleedthrough, substandard margins, and improper alignment can adversely affect reproduction.

In the unlikely event that the author did not send UMI a complete manuscript and there are missing pages, these will be noted. Also, if unauthorized copyright material had to be removed, a note will indicate the deletion.

Oversize materials (e.g., maps, drawings, charts) are reproduced by sectioning the original, beginning at the upper left-hand corner and continuing from left to right in equal sections with small overlaps. Each original is also photographed in one exposure and is included in reduced form at the back of the book.

Photographs included in the original manuscript have been reproduced xerographically in this copy. Higher quality 6" x 9" black and white photographic prints are available for any photographs or illustrations appearing in this copy for an additional charge. Contact UMI directly to order.

UMI

A Bell & Howell Information Company
300 North Zeeb Road, Ann Arbor MI 48106-1346 USA
313/761-4700 800/521-0600

An Application of Potential Vorticity Inversion to the Position Forecast Problem of Hurricane Opal

by

John M. Henderson

A thesis submitted to the Faculty of Graduate Studies and Research in partial fulfilment of the requirements of the degree of Master's of Science

Department of Atmospheric and Oceanic Sciences
McGill University
Montreal, Quebec

 March 1997

Abstract

Accurate forecasting of hurricane motion is required to prepare for hurricane landfall. The underpredicted acceleration of Hurricane Opal by the National Centers for Environmental Prediction's (NCEP) operational eta model during landfall and over-land passage is investigated using quasi-geostrophic potential vorticity (QGPV) inversion. We identify and explain model errors in the evironmental steering flow using a systematic procedure including removal of Opal's cyclonic circulation that builds upon previous work.

The eastern ridge associated with the anticyclonic QGPV was persistently forecasted too weak and too distant from Opal, though the forecast of this feature improved at shorter ranges. The anticyclonic contribution to the retrieved flow increased from -11% of the observed vector (inhibiting the motion) to 15% (aiding the motion). This increase of 3.8 m s^{-1} is alone sufficient to explain the slow forecast.

The eta forecasts likely did not sufficiently resolve the advection downstream of storm outflow and subsequent ridge building. This error propagated through the forecast cycle and prevented phase-locking with the ridge and increased flow. Representation of the ridge improved following advection of the outflow over the more dense U.S. upper air network.

This study emphasizes the need for accurate upper-air analyses and offers a real-time application of QGPV inversion that decomposes the steering flow. The need for further research into the intimate relationship between storm intensity and subsequent storm track is stated.

Résumé

Il est nécessaire de prévoir de façon précise la trajectoire des ouragans afin de se préparer pour leur arrivée à l'intérieur des terres. La sous-estimation de l'accélération de l'ouragan Opal par le modèle opérationnel eta, du National Centers for Environmental Prediction, lors de son arrivée puis au cours de son passage sur le continent est étudiée en utilisant la technique d'inversion de tourbillion potentiel quasi-géostrophique (TPQG). On identifie et explique les erreurs du modèle dans les vents directionnels en utilisant une méthode systématique qui soustrait la circulation cyclonique d'Opal et qui marque un progrès sur les résultats d'études antérieures.

La crête orientale associée au TPQG anticyclonique a systématiquement été sous-estimée et prévue trop loin d'Opal. Par contre, la prévision de la crête était meilleure a plus court terme. La contribution anticyclonique du vent calculé a augmenté de -11% du vecteur observé (contre le mouvement de l'ouragan) à 15% (avec le mouvement). Cette augmentation de 3.8 m s^{-1} est suffisante pour expliquer la prévision lente.

Les prévisions du modèle eta n'ont probablement pas suffisamment capté l'advection en aval des vents sortant de l'ouragan et l'augmentation de la crête. Cette erreur s'est propagée dans la prévision et a empêché le couplage de phase entre la crête et la circulation augmentée. La crête a été mieux captée une fois que la circulation sortante de l'ouragan a été advectée au-dessus du dense réseau de détection des Etats-Unis.

Cette étude met l'emphase sur l'importance de réaliser des analyses précises en altitude et propose une application réel de l'inversion TPQG qui décompose la circulation environnementale.

Table of Contents

Acknowledgments

I wish to thank my supervisor, Dr. John Gyakum, who allowed me the freedom to select such an interesting and relevant topic as Hurricane Opal. His guidance and timely support has kept me focussed and provided me with great opportunities to expose my work to the research community.

Dr. Gary Lackmann, a postdoctoral student of Dr. Gyakum, provided the motivation for this study even as Opal was making history in Florida. He has given unconditional help whenever needed and irreplaceable technical advice that made this work possible. Even after leaving for the State University of New York (SUNY) in Brockport in 1996, Gary has continued as an unofficial supervisor through to the completion of this work. I wholeheartedly thank him for his support.

I am grateful for the use of the QGPV inversion code, written by Greg Hakim of SUNY Albany and provided by Gary Lackmann, that was invaluable to this project. I thank Marco Carrera for reviewing the technical style of my thesis, providing computer code and for many a lively discussion to which our office neighbours can attest! I also thank Werner Wintels for enlightening discussions, Will Cheng and Rick Danielson for technical support and Alex Fischer for a constructive review. The translation of the abstract into French by Dov Bensimon and Paul Vaillancourt is much appreciated. To my parents, thank you for giving me the opportunity and ability to follow something I enjoy.

I acknowledge the European Centre for Medium Range Weather Forecasting for providing data through the National Center for Atmospheric Research and for funding from the Natural Science and Engineering Research Council.

Chapter 1

Introduction

1.1 The Problem of Hurricane Forecasting

The allure of the barrier islands of the United States' Atlantic and Gulf of Mexico coasts is tempered by the persistent threat of tropical cyclones during the summer and autumn seasons. A generation of coastal residents is now paying for their complacency as annual damage estimates reach into the billions of dollars. Intense hurricanes are making frequent landfall in the 1990s and awakening a coastal population largely without first-hand experience of a major hurricane. Coastal areas of South Carolina (Hurricane Hugo in 1989) and southeastern Florida (Hurricane Andrew in 1992) have recently suffered extensive damage from the storm surges and strong winds that gusted to nearly 80 m s^{-1} (Wakimoto and Black 1994; Willoughby and Black 1996). Refer to Fig. 1.1 for the locations of geographical references. As well, six intense hurricanes (maximum sustained winds of at least 50 m s^{-1}; see Table 1.1) formed in the Atlantic ocean in 1996; Hurricane Fran made landfall at this intensity in South Carolina. With the continuing rapid increase in coastal population and development (Sheets 1990), the need for accurate and timely prediction of hurricane landfall is becoming more and more apparent.

Fig. 1.1. Locator map for references in the text.

Table 1.1

Category	Maximum Sustained Winds ($m\ s^{-1}$)	Central Pressure (hPa)
1	33-43	> 980
2	44-49	965-980
3	50-58	945-964
4	59-70	920-944
5	> 70	< 920

The Saffir-Simpson Hurricane Damage-Potential Scale (Simpson, 1974).

Forecasts of tropical cyclone landfall by the National Hurricane Center (NHC, part of the Tropical Prediction Center) continue to save lives since the mean annual number of hurricane related fatalities is decreasing (Sheets 1990). The potential for catastrophe, however, from individual intense hurricanes is increasing because of coastal population growth and development. The 20-30 h needed to evacuate the most hurricane-prone areas (Brinkmann 1975), such as the Galveston and Tampa Bay areas and the southeast Florida coast (AMS 1986a), is significantly longer than the NHC's goal of twelve daylight hours of warning time. Compounding this problem is the public's misconception of how long is needed for evacuation (AMS 1986a). With increasing coastal population, the precise location of landfall must also be determined even earlier for complete evacuation to be possible. However, the warning areas that now average 500 km in length and cost more than 50 million dollars to effect (Sheets 1990), must remain small, less credibility and public response deteriorate. Note that in this study, the term 'hurricane' is used to represent all intensities of tropical cyclones, unless reference is made to specific storms or the term is noted otherwise.

The NHC continues to provide improving forecasts of hurricane track and intensity. The average distance between a NHC forecast and the observed storm position (termed the forecast error) has decreased by 14% over the last 20 years (AMS 1993). For the decade 1976-1985, forecast errors for 24, 48, and 72-h forecasts were 215 km, 459 km and 687 km (AMS 1986b), respectively. The respective 12, 24, 48, and 72-h forecasts for 1982-1991 were still 100 km, 193 km, 383 km and 573 km (AMS 1993), even with these improvements. Errors of this size make the forecast location of landfall less credible to the public, as well as financially costly, since evacuation of 2/3 of the warned area is unnecessary in terms of realized damage (AMS 1993). Meanwhile, forecasts of storm intensity, while improving, are still only slightly better than those based on persistence and climatology. Large intensity changes are occasionally not predicted which is of great concern when landfall is expected within 24 h (AMS 1993).

Improved numerical guidance will continue to result in better hurricane forecasts. Meanwhile, evaluation of past model performance, especially poor model performance,

can be illuminating. The statistical and dynamical hurricane track and intensity models run by the NHC have previously been described and evaluated (Neumann and Pelissier 1981; DeMaria et al. 1990). However, it is the operational regional and global models run by the NCEP that provide primary guidance to the NHC. Sheets (1990) anticipated that these models, developed primarily for the baroclinic mid-latitudes, would soon show skill (with respect to climatology and persistence) in the prediction of tropical cyclones. As such, knowledge of the strengths and weaknesses of the models is important, especially when the storms are in their landfall or post-landfall transitionary stages. This study evaluates poor forecasts by the NCEP (then the National Meteorological Center) short-range operational eta model (Mesinger et al. 1988; Black et al. 1993; Rogers et al. 1995) for Hurricane Opal in October 1995.

1.2 Thesis Objectives and Outline

We chose Hurricane Opal as a case study for three reasons. First, numerical model guidance underestimated the storm's forward motion, which resulted in official NHC forecast errors at 48 and 72 h being larger than the prior 10-year average. The average 12, 24, 36, 48 and 72-h NHC forecast errors for Hurricane Opal were 77 km, 188 km, 296 km, 425 km and 600 km, respectively. Specifically, the forecast storm positions by the eta model were especially poor (see Fig. 1.2). Second, Opal rapidly and unexpectedly intensified in the early morning hours of 4 October to category-4 strength (see Table 1.1) on the Saffir/Simpson scale (Simpson 1974), just 12 h prior to landfall. The critical element of issuing watches and warnings to maximize the public's response was a challenge in this case. Third, Opal was an intense storm whose forward motion continued to increase through landfall, with strong winds and heavy rainfall well inland. The storm was becoming extratropical in a mid-latitude baroclinic environment during the period of study. The eta model provides guidance for this region and so its performance is invaluable to local forecasters shouldered with the responsibility of issuing inland

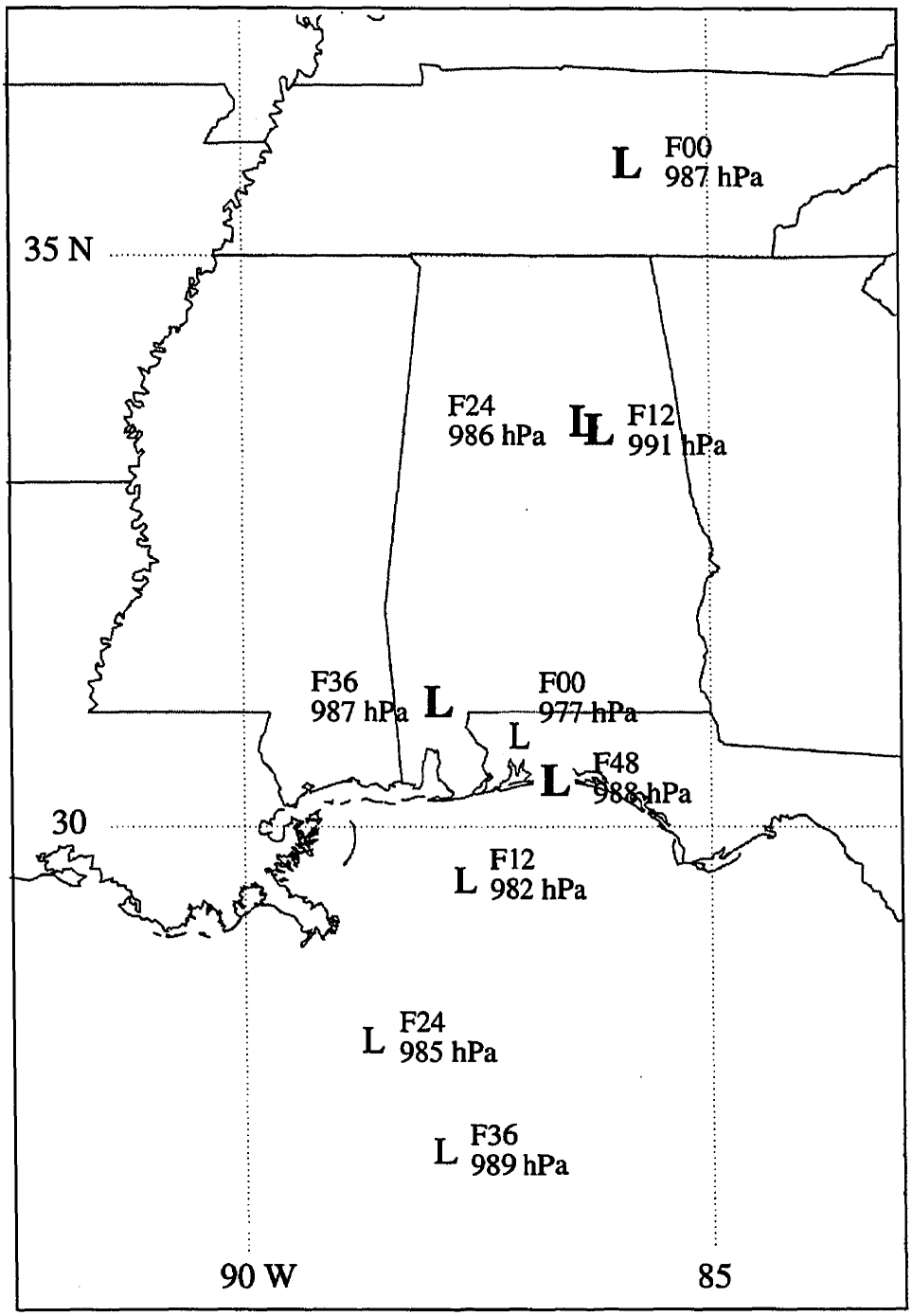

Fig. 1.2. Eta model forecast positions of Hurricane Opal, valid at 0000 UTC (light symbols) and 1200 UTC (bold symbols) 5 October 1995. The lead times of the position forecasts are given after the letter 'F'. For example, the 36-h forecast issued at 1200 UTC 3 October and valid at 0000 UTC 5 October is positioned farthest south. Forecast sea level pressures are also given.

forecasts and warnings.

The goals of this study are:

1. To document the synoptic environment of Hurricane Opal.

2. To illustrate that quasi-geostrophic potential vorticity (QGPV) is useful for determining the steering flows of hurricanes by carrying out potential vorticity inversion.

3. To evaluate the steering flows obtained from two different model analyses - the European Centre for Medium Range Weather Forecasting (ECMWF) and the eta.

4. To compare the steering flow obtained from the eta model's 12, 24, 36 and 48-h forecasts to those from the above analyses. We identify misrepresented synoptic features responsible for differences between the forecast and analyzed steering flows. The inversion of model forecasts to determine the cause of poor forecasts has not appeared in the literature to the best of the author's knowledge.

5. To identify the poorly simulated physical processes that resulted in misrepresentation of the synoptic features.

Chapter 2 presents a brief history of Hurricane Opal to familiarize the reader with the history of the storm. A synoptic overview describes the storm's environment using Ertel's potential vorticity and qualitatively identifies the relevant synoptic features contributing to the southerly environmental flow over the storm. Chapter 3 reviews traditional and potential vorticity definitions of the hurricane steering flow in the literature and introduces the potential vorticity method used in the present study. Chapter 4 defines quasi-geostrophic potential vorticity, details the current inversion method, and compares and contrasts against established methods that have appeared in the literature. Chapter 5 presents the contributions to the steering flow by synoptic features (retrieved through the inversion in chapter 4). The poorly represented contributions are then identified and plausible physical explanations are given. Conclusions are drawn in chapter 6.

Chapter 2

Hurricane Opal and the Synoptic Environment

This chapter gives an overview of Hurricane Opal and the synoptic pattern in which the storm was embedded. The goal is to familiarize the reader with the relevant features steering the storm. Section 2.1 describes the life cycle of Opal. Section 2.2 introduces Ertel's (1942) potential vorticity (EPV) to facilitate an EPV description in later sections of the synoptic features that contributed to a southerly advective component of the steering flow.

2.1 The Life of Hurricane Opal

Figure 2.1 is a reproduction of the best-track path of Hurricane Opal from the NHC's Preliminary Report for Hurricane Opal (NHC 1995). The precursor to Opal, Tropical Depression 17, formed at 1800 UTC 27 September 1995 near the east coast of the Yucatan Peninsula of Mexico and drifted slowly into the northern part of the peninsula over the next 66 h. The depression was upgraded to Tropical Storm Opal at

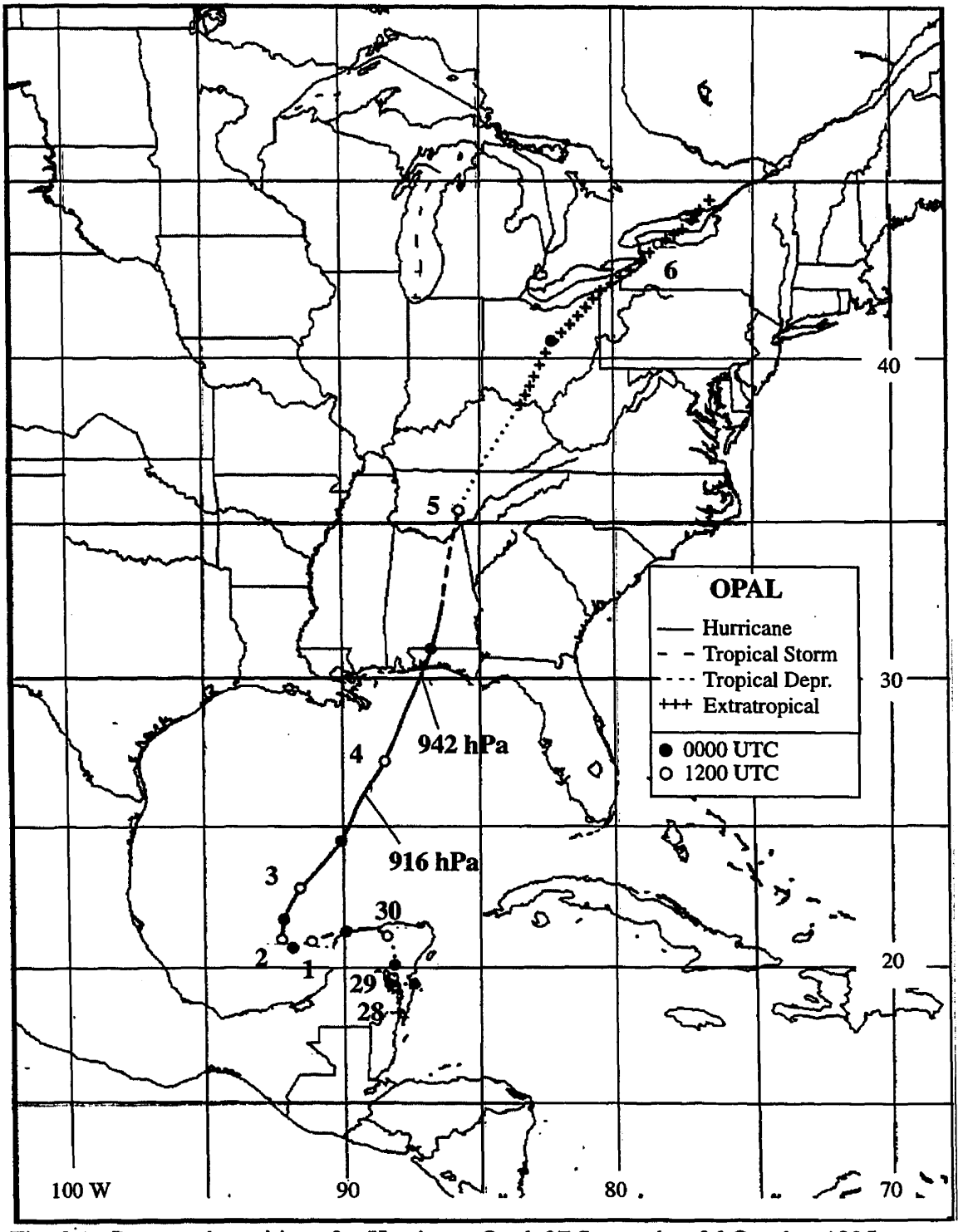

Fig. 2.1. Best track positions for Hurricane Opal, 27 September-06 October 1995 (National Hurricane Center 1995).

1200 UTC 30 September 1995 and drifted for 48 h into the Gulf of Mexico in response to weak easterly, then east-northeasterly, steering flow. At 1200 UTC 2 October, coincident with Opal reaching hurricane status, the upper-level flow over the storm changed significantly as the baroclinic westerlies became influential. Opal turned to the north then north-northeast and intensified slowly, but steadily, despite the increased vertical shear. At 1200 UTC 3 October, Opal was located over the southern Gulf of Mexico with a central pressure of 968 hPa and maximum sustained surface winds estimated at 40 m s^{-1}.

According to the NHC Preliminary Report, rapid deepening commenced at 1200 UTC 3 October in response to warmer surface water, well established upper-level outflow and constriction of the eyewall as part of a replacement cycle. A larger, concentric eyewall, whose radius decreases with time, often forms in intense hurricanes. Fluctuations in storm intensity occur as the larger eyewall replaces the existing eyewall (Willoughby et al. 1982). Opal's lowest central pressure of 916 hPa was observed at 0945 UTC 4 October. This pressure fall of 42 hPa over 12 h makes Opal a 'rapid deepener' according to Holliday and Thompson's (1979) criterion of 42 hPa in 24 h for their study of storms in the western North Pacific. This large pressure fall (53 hPa over 24 h), however, is not unprecedented (see Holliday and Thompson for examples). At 1000 UTC 4 October 1995, while approximately 450 km south-southwest of Pensacola, Florida, Opal had sustained surface winds estimated at 65 m s^{-1} and was moving towards the Florida panhandle at 8.9 m s^{-1} (calculated using a 12-h finite difference from NHC best-track data; see details later in the text).

Landfall occurred at approximately 2200 UTC 4 October several kilometres west of Hurlburt Field (HRT), Florida. The landfall central pressure was estimated at 942 hPa with sustained surface winds locally of 50 m s^{-1}. The minimum sea-level pressure observed was 948 hPa at 2302 UTC at the intersection of Interstate 10 and East Bay. Peak observed sustained winds of 36 m s^{-1}, with gusts to 64 m s^{-1}, were reported by HRT near the time of landfall. Opal was moving to the north-northeast at about 10 m s^{-1}.

Post-landfall sustained winds weakened as the storm accelerated inland, likely because of the removal of surface latent heating (Miller 1964). However, strong wind

gusts to 40 m s^{-1} (MXF, Maxwell AFB, Montgomery, Alabama) were still felt well inland because of the rapid motion of the storm. Opal was a tropical storm by 0600 UTC 5 October with sustained winds of 26 m s^{-1} while the storm was over central Alabama. By 1200 UTC, 6 h later, the maximum sustained winds were 15 m s^{-1} and Opal had been downgraded to a tropical depression.

By 1800 UTC, the surface pressure gradient to the north of the remnants of Opal was beginning to increase as the storm approached a surface high pressure area over the upper Great Lakes. In response, the sustained surface wind speed increased to 21 m s^{-1} even though the storm's central pressure continued to rise. The strongest winds at this time were occurring over and near Lakes Erie and Ontario with gusts to nearly 30 m s^{-1}. Heavy rainfall accompanied the storm from Florida to the Great Lakes where Toronto (YYZ) received 78.6 mm over a 24-h period.

Opal maintained a fairly steady heading (Fig. 2.1) from 1200 UTC 2 October until the end of the best-track path over southern Ontario on 6 October. This suggests that the storm was embedded in a slowly changing synoptic-scale steering flow for the duration of the recurvature northward. Table 2.1 gives a summary of the observed locations and forward speeds of Hurricane Opal at three times during recurvature. The movement of the storm is calculated using 12-h finite differences from best-track data, thus minimizing the noise associated with raw fixes (Jarrell 1993). This time period, according to Jarrell, is more than adequate to accurately represent the motion of well-organized tropical cyclones.

Nine deaths were directly associated with Opal in the United States, all due either to falling trees or tornadoes. It is noteworthy that the storm surge, usually the most deadly facet of a hurricane, did not result in any deaths.

Table 2.1

Date/time	Location	Motion
0000 UTC 4 October	24.5° N 90.1° W	7.2 m s^{-1} from 211°
0000 UTC 5 October	31.0° N 86.8° W	11.3 m s^{-1} from 197°
1200 UTC 5 October	35.4° N 85.7° W	14.8 m s^{-1} from 202°

NHC location and 12-h finite difference best track vector motion for Hurricane Opal.

2.2 The Synoptic Environment

2.2.1 Potential Vorticity

Let us use Ertel's potential vorticity (EPV) (1942) to facilitate the identification of the synoptic features of the environment in which Opal was embedded. EPV is defined as:

$$Q = \frac{\Omega \cdot \nabla \theta}{\rho} \qquad (2.1)$$

where Ω is the three-dimensional absolute vorticity vector, $\nabla\theta$ the three-dimensional gradient of potential temperature and ρ the density of the air. A good approximation for the full EPV in the hydrostatic atmosphere (Bosart and Lackmann 1995) is:

$$Q = -g\frac{\partial\theta}{\partial p}\left(f + \frac{\partial v}{\partial x} - \frac{\partial u}{\partial y}\right) + g\left(\frac{\partial v}{\partial p}\frac{\partial\theta}{\partial x} - \frac{\partial u}{\partial p}\frac{\partial\theta}{\partial y}\right). \qquad (2.2)$$

An exhaustive review of potential vorticity is given by Hoskins et al. (1985, hereafter referred to as HMR). It has been observed that the vertical gradient of EPV increases dramatically from the troposphere to the stratosphere because of the strong static stability in the latter (the stratosphere represents a 'reservoir' of high EPV). Typical values of tropospheric EPV are 0.5 to 1.0 PVU (where 1 Potential Vorticity Unit (PVU) = 10^{-6} K m^2 s^{-1} kg^{-1}), while stratospheric values are an order of magnitude higher. The position of the discontinuity is determined primarily by advection following the three-dimensional motion of the air. Hoerling et al. (1991) noted that EPV values of 1-3 PVU can be used to qualitatively define the location of the tropopause. We define the *dynamic* tropopause as the 1.5-PVU surface following Davis and Emanuel (1991), Huo et al. (1995), Molinari et al. (1995), Bresky and Colucci (1996), Merrill and Velden (1996) and Wu and Kurihara (1996).

Upper tropospheric short-wave troughs and jet features maintain their maximum

amplitude at the tropopause (Bosart and Lackmann 1995). Tropopause maps, therefore, summarize concisely the dynamic features of the upper levels. The choice of the pressure level that will intersect the features of interest is not a concern since the height (e.g., pressure and potential temperature, as well) varies, according to these upper features, on the tropopause.

While the 1.5-PVU surface contains physical significance in terms of a vertical change in the static stability gradient, the 0-PVU surface is important in terms of inertial stability. When EPV becomes negative, the flow becomes inertially unstable. This phenomenon is uncommon in the atmosphere (because of relatively instantaneous attempts to restore inertial stability) but is seen in isolated areas on the equatorward side of jet streams (Hoerling et al. 1991). As well, Jordan (1952) believed local areas of vanishing EPV were likely in the upper-level outflow of hurricanes.

HMR describe the three dimensional flow associated with individual EPV *anomalies* (with respect to a slowly-changing background state), which, when added to the background state, completely describe the state of the atmosphere. Positive anomalies induce cyclonic gyres while negative anomalies induce anticyclonic gyres. (The idea of potential vorticity partitioning and induced flow will be explained in detail in chapter 4 using quasi-geostrophic potential vorticity).

HMR further identify two attractive principles of EPV. The first is that EPV is conserved following isentropic flow in the absence of diabatic heating and friction. EPV is thus an adequate tracer (potential temperature, θ, is conserved) for upper tropospheric and stratospheric air motion since heating is generally localized and friction is small. Advection then is the principle method by which there are local potential vorticity changes.

In contrast, latent heating plays a large role in increasing the local EPV of the lower and middle levels of the troposphere. EPV is generated below the level of maximum latent heating and dissipated above, owing to increased and decreased static stability, respectively. In the infrequent case of hurricanes and their associated convection, there will be a decrease over time of EPV in the hurricane's upper tropospheric anticyclone. The tropopause in this region will then be found at higher

heights (higher θ_T, lower p_T) as EPV decreases and the 1.5-PVU surface rises. Bosart and Bartlo (1991) observed this latent heating EPV dipole (a maximum at lower levels and minimum at upper levels) for Tropical Storm Diana (1984).

The second principle states that given the three-dimensional distribution of EPV, boundary conditions and an appropriate balance equation between the height (Φ) field and streamfunction (Ψ) (and wind field), all dynamical and thermodynamical meteorological quantities can be retrieved through a process called inversion. This second tenet of potential vorticity thinking will be elucidated further in the context of Hurricane Opal in chapters 4 and 5.

Dynamic tropopause maps during Hurricane Opal's recurvature will be presented in the following sections.

2.2.2 Data Set

The fields to be presented have been calculated from European Centre for Medium Range Weather Forecasting (ECMWF) analyses, available every 6 h, but presented here only for 0000 UTC 4 October and 0000 UTC and 1200 UTC 5 October 1995. The ECMWF analyses (Trenberth 1992) consist of height, temperature, relative humidity, observed wind and vertical velocity on a 1.125° by 1.125° grid, interpolated to a 1° by 1° latitude-longitude grid, on the following pressure levels (in hPa): 1000, 925, 850, 700, 500, 400, 300, 250, 200, 150, 100 and 50. Data were interpolated at 50-hPa intervals from 1000 hPa to 50 hPa, hydrostatically balanced and imported into the Generalized Meteorological Analysis Package (GEMPAK) software (Koch et al. 1983) for storage, analysis and display.

2.2.3 EPV Dynamic Tropopause and Lower Tropospheric Maps

Using (2.2) to calculate EPV, we present four-panel maps (similar to those of Hakim et al. 1995; see also Bosart and Lackmann 1995) in Figs. 2.2, 2.3 and 2.4 for 0000 UTC 4 October, 0000 UTC 5 October and 1200 UTC 5 October, respectively. As can be seen in Fig. 2.2a and Fig. 2.2b, a large trough over the central U.S. has two embedded shortwave troughs (localized lower tropopause potential temperature, θ_T, and higher tropopause pressure, p_T); the eastern trough is located over eastern Missouri while the western one is just entering the northwest corner of the domain.

Note that the dynamic tropopause is determined by the first 1.5-PVU surface when searching vertically from the 50-hPa level toward higher pressures. Regions of tropopause folds (Pauley et al. 1996; Lamarque and Hess 1994) are, in general, identified by different values of p_T when searching downward from the top and upward from the bottom. Areas where Δp_T>200 hPa are 'ringed' because the large pressure difference between the multiple 1.5-PVU levels is likely due to latent heating.

The eastern shortwave trough is advected northeastward by the geostrophic flow in Fig. 2.2a while the western shortwave is moving southeastward. An upper level ridge and warm tropical air mass with a high tropopause is situated over the southeastern U.S. Opal is located over the central Gulf of Mexico well within this ridge. The subtropical jet over southern Texas forms the southern end of the eastern shortwave and defines the northern limit of the tropical air, while a closed upper level cold low well to the east of the Bahamas (just east of the domain of the map, not shown) defines the eastern limit. The proximity of this low results in a strong anticyclonically-curved northerly flow on the dynamic tropopause off the southeast coast of the U.S. The low is in a favourable position to enhance the outflow from Opal, as noted for previous tropical-synoptic interaction patterns by Sadler (1976); indeed, there is a large anticyclonic gyre generally to the east of Opal in the wind field (Fig. 2.2a) associated with a region of locally lower upper-tropospheric EPV. The contouring strategy of Figs. 2.2a and 2.2b draws attention to the tropopause topography in the vicinity of Opal where θ_T is 361 K, indicative of

Fig. 2.2. Dynamic tropopause and lower troposphere EPV map at 0000 UTC 4 October 1995. Panel (a) is a plot of potential temperature on the tropopause, θ_T, contoured every 10 K (solid) for multiples of 10 K (i.e., 300 K, 310 K, etc). Contours every 10 K are also plotted for 365 K and above (dashed). Geostrophic f-plane ($f = 10^{-4}$ s^{-1}) winds on the tropopause are shown (one half barb equals 2.5 m s^{-1} while one pennant equals 25 m s^{-1}). This notation will be used throughout the study. Panel (b) is a plot of pressure on the tropopause, p_T. Regions of tropopause folds of varying depths (in hPa, as specified by the shading scheme) are identified. The contour interval (solid) is every 50 hPa down to 150 hPa and (dashed) every 10 hPa below. Panel (c) is a plot of the 850-700 hPa layer-average EPV, contoured every 0.5 PVU, and shaded as indicated. Layer-averaged geostrophic winds are also plotted. Panel (d) is a plot of 850 hPa geopotential height (every 3 dam, solid), relative humidity (%, shaded as shown) and 1000-850 hPa thickness (every 3 dam, dashed). The positions of selected surface features are given. Opal is located in the central Gulf of Mexico.

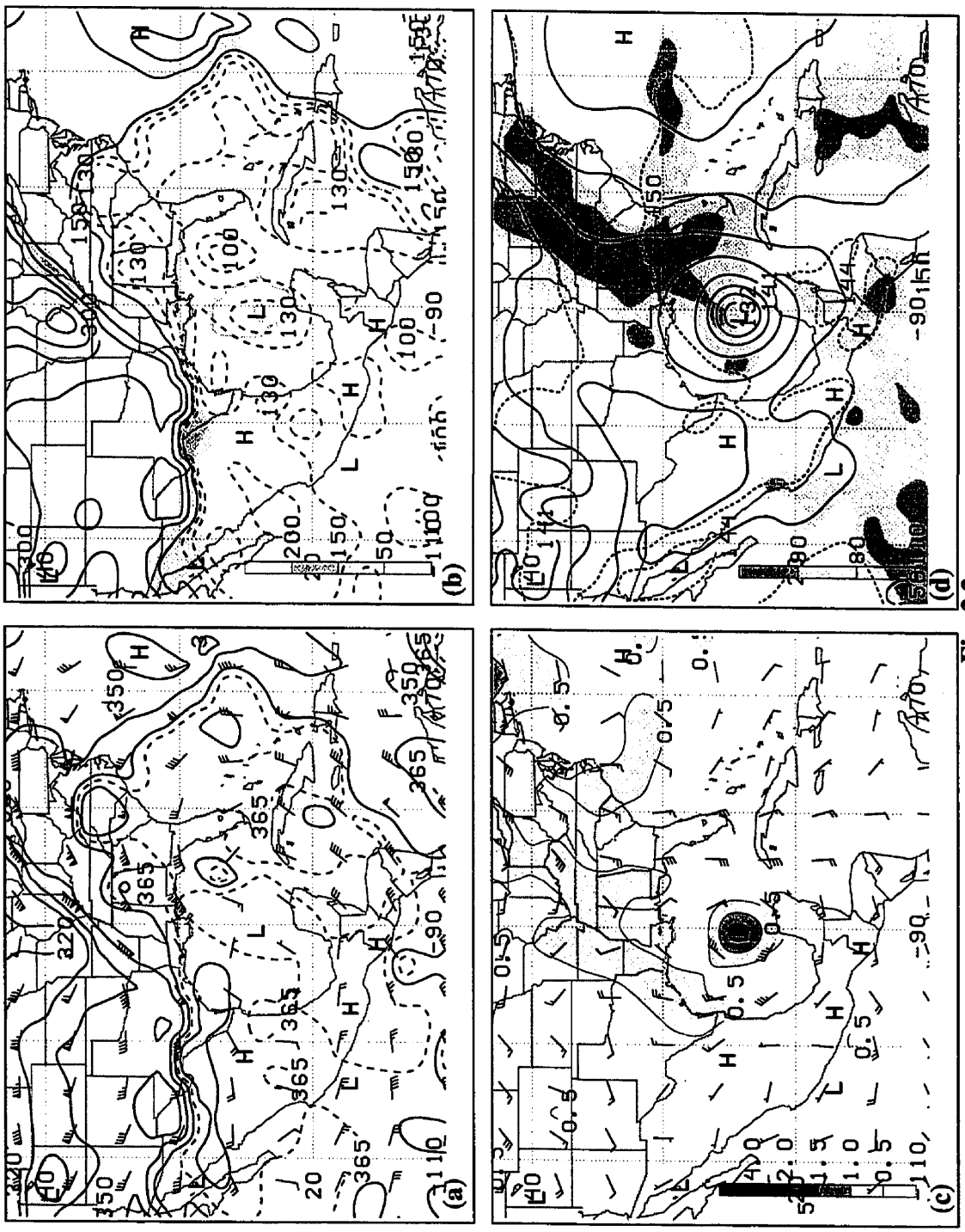

Fig. 2.2

the tropical air mass in which Opal is embedded.

The location of Opal in Fig. 2.2c is marked by a strong low level EPV maximum. This is typically a result of diabatic potential vorticity redistribution in a region of latent heat release (Raymond 1992). Note the high levels of vorticity inferred from the cyclonic gyre accompanying the local EPV maximum. The other readily noticeable feature is the expansive area of higher EPV from near Brownsville, Texas (BRO) to Lake Erie. This is also likely the result of latent heating, the legacy of a slowly moving cold front that had produced widespread rainfall in this region over the preceding couple of days. A poor forecast (not shown) of this low level local maximum (and thus prior rainfall) and the associated cyclonic wind gyre may have been influential in the poor forecast of Opal (see chapter 4).

Areas of cloud and precipitation associated with this cold front extend northward from the northeastern Gulf (Fig. 2.2d). It is noteworthy that the size of Opal's circulation exceeds the criteria of Merrill (1984) for a 'large' Atlantic storm; the radius of the outer closed sea-level pressure isobar (not shown, but the 850-hPa heights are a good proxy) is greater than 4° latitude. Part of this circulation is advecting warm air northward between the storm and a large high pressure area just east of the 70th meridian.

Winds on the tropopause at 0000 UTC 5 October (Fig. 2.3a) have advected the well developed western shortwave into southeastern Colorado and the upper level ridge farther northeast. Opal is located over the panhandle of Florida, again 'ringed' by latent heating effects. The upper low has drifted southwestward (a common motion for such a feature (Whitfield and Lyons 1992)) to be east of the Bahamas with the tropopause now depressed to a pressure larger than 300 hPa (Fig. 2.3b). As a result, winds between the low and the ridge have increased to 35 m s^{-1}, enhancing general upper air motion away from Opal. Note that θ_T in the vicinity of Opal has increased over the past 24 h to 370 K. The storm is now completely embedded in a region of θ_T above 370 K, unlike 24 h earlier. Based on the diffluent pattern of tropopause winds around Opal at 0000 UTC 4 and 5 October, we believe that advection alone cannot explain the observed θ_T field at 0000 UTC 5 October. Latent heating, in the form of Opal's low EPV upper outflow,

Fig. 2.3. As in Fig. 2.2, but for 0000 UTC 5 October 1995. Opal is located over the Florida panhandle.

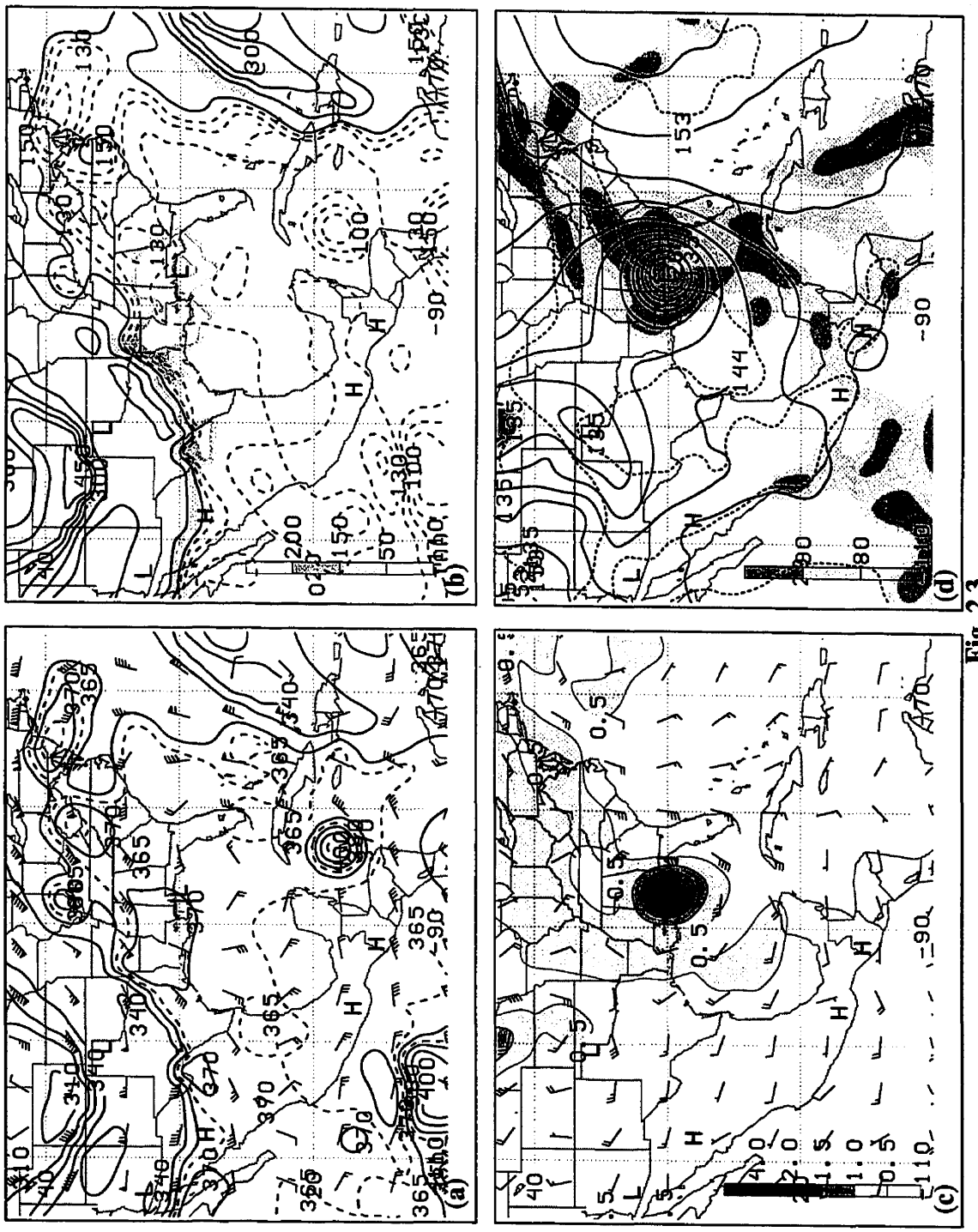

Fig. 2.3

may be building the downstream ridge throughout the period including landfall (2200 UTC 4 October). The upper level anticyclone directly associated with Opal lies to the southeast of the storm at 100 and 150 hPa (not shown); it then weakens and merges with the downstream ridge to the northeast at lower levels in the upper troposphere (200-300 hPa). Opal's outflow pattern at 0000 UTC 4 October and 0000 UTC 5 October is very similar to Merrill's (1988) Atlantic Type I, with strong anticyclonic curvature of the outflow jet that eventually merges with the easterlies. A trough in the mid-latitude westerlies is advecting the upper level low potential vorticity outflow from Opal downstream into the ridge, as seen by Wu and Kurihara (1996) for Hurricane Bob.

Figure 2.3c shows locally-higher EPV over the eastern U.S. As well, rainfall over the past 24 h has occurred to the west and southwest of Opal. This may be partially precipitation that fell when Opal passed through this region.

Figure 2.3d shows increased warm air advection east of Opal in a strengthening southerly flow. This is likely aiding in the generation of orographic precipitation over the southern Appalachian mountains. A surface extratropical cyclone associated with the upper level shortwave can be seen in northern Texas. Drier, cooler air is being incorporated into Opal's circulation from the west and north. This is seen by the sub-saturated air and lower thicknesses to the west of the storm's centre.

Opal has accelerated into eastern Tennessee by 1200 UTC 5 October (Fig. 2.4b) where its latent heating effects merge with the deep fold along the subtropical jet in the Gulf Coast states. This is a consequence of the shading strategy for tropopause folds and the limitations of the synoptic-scale dataset. (The resolution of the ECMWF gridded data is originally 1.125° by 1.125°). The extension of the ringed area over Lousiana, Mississippi and Alabama, is, upon closer examination, not due to latent heating. Figure 2.5 is a northwest-to-southeast vertical cross-section through the extratropical cyclone, tropopause fold and eastern upper low; the deep (>200 hPa from the bottom to the top occurrence of 1.5 PVU), dry (relative humidities less than 25 %) tropopause fold on the subtropical jet is clearly seen. The low and mid-level moist local EPV maximum of Opal is north of this cross-section and is clearly separate from the tropopause fold. Warm tropical air continues to be advected northeastward by the subtropical jet but the ridge has

Fig. 2.4. As in Fig. 2.2, but for 1200 UTC 5 October 1995. Contours above 380 K have been suppressed in panel (a). Opal is positioned over Tennessee. The location of the cross-section in Fig. 2.5 is shown in panel (b).

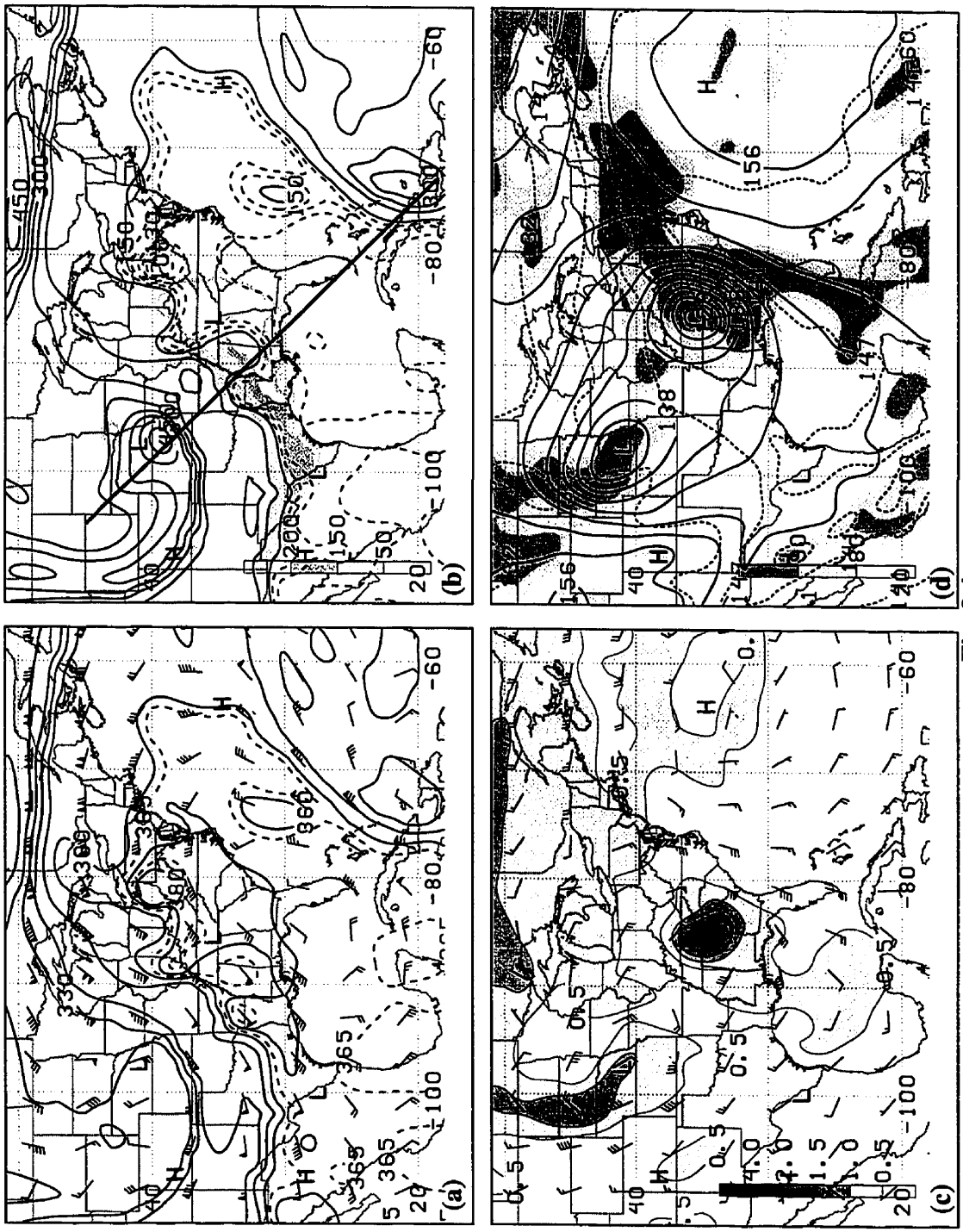

Fig. 2.4

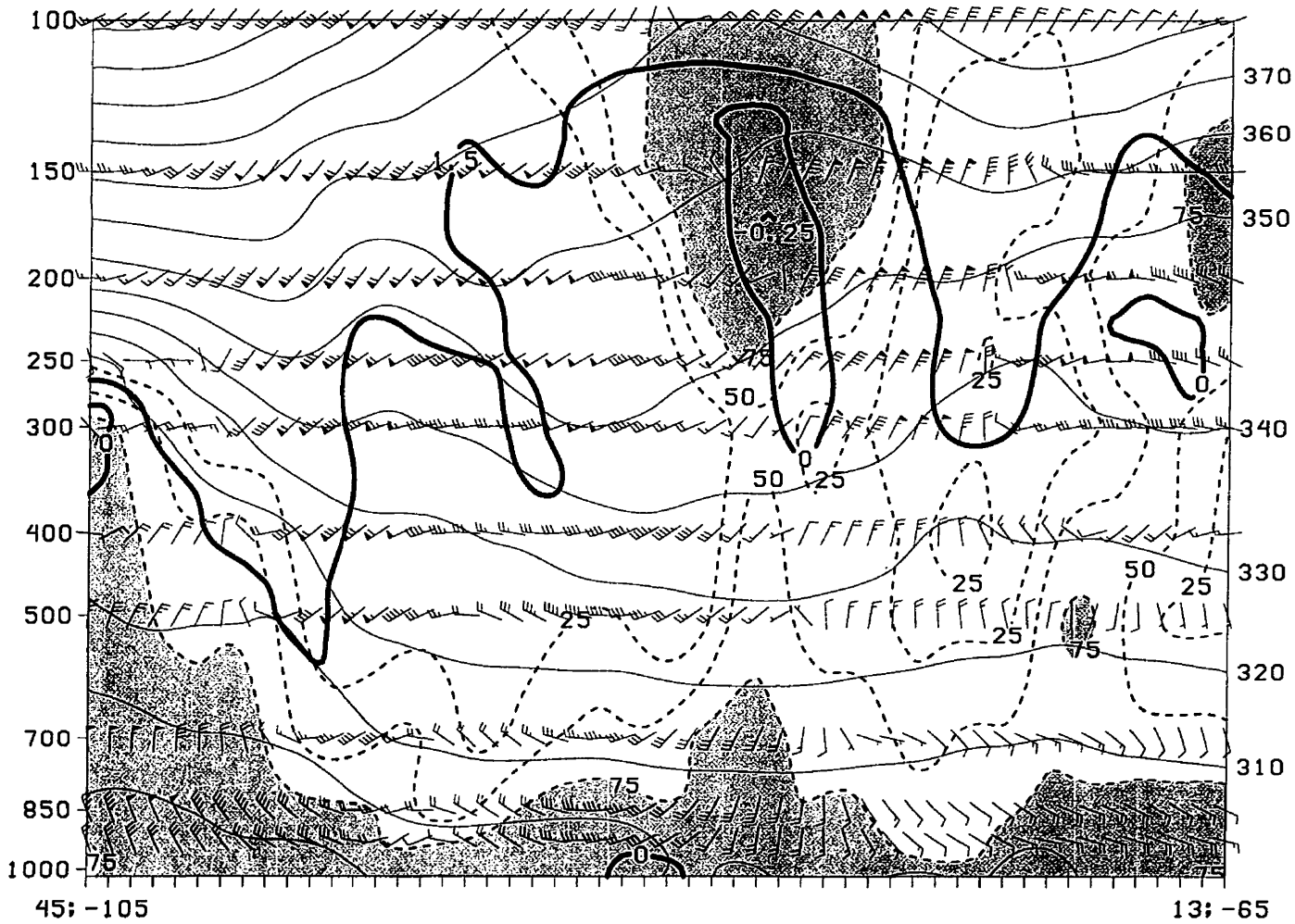

Fig. 2.5. Cross-section at 1200 UTC 5 October of EPV (-0.25, 0 and 1.5 PVU plotted in bold contours), relative humidity (every 25% in dashed, shaded above 75%), potential temperature (every 10 K in thin contours) and observed winds (notation as in Fig. 2.2a). Cross-section extends from 45° N 105° W to 13° N 65° W.

become more elongated northeast-southwest as the upper level low digs southwestward north of Haiti. Opal likely continues to build this downstream ridge (Fig. 2.4a), with θ_T in the vicinity of the storm having increased to 375 K. The 365 K contour now covers all of the southeastern U.S. while the 370 K contour has expanded over the mid-Atlantic and the northeastern Gulf states. [A localized area of θ_T above 400 K in eastern Ohio (contour not shown for clarity) is associated with deep nocturnal convection]. Note that the increase in tropopause potential temperature near Opal is greater than can be explained by the combined effects of advection and uncertainty in the ECMWF analysis (which is a smoothed representation of the eta analysis).

Opal's outflow at this time is merging with the westerlies, eventually riding over the downstream ridge well to the northeast of the storm. Immediately downstream of the ridge is the upper low. The western shortwave trough has strengthened (p_T now above 500 hPa) and moved to northeastern Kansas. Its surface circulation has also intensified and now lies in southeastern Nebraska. A low level maximum of EPV (Fig. 2.4c), independent of Opal and colocated with clouds and precipitation (Fig. 2.4d), is seen over the Plains states associated with the western low. As well, a zone of low level confluence over Florida and strengthening warm advection over the mid-Atlantic states is resulting in extensive clouds and precipitation. Frontogenesis is occurring to the east of Opal as southerly winds advect tropical air towards the baroclinic zone that lies over the Great Lakes and northeastern U.S.

2.2.4 Discussion

The placement of a middle latitude trough to the northwest and a ridge to the east was conducive to a general southerly flow over Opal. From 0000 UTC 4 October to 1200 UTC 5 October, the distance between these two features decreased and Opal responded to the increased pressure gradient and accelerated towards higher latitudes. The relative contributions to the steering flow by the trough and ridge, however, cannot

be determined solely from conventional analyses. Thus, chapter 4 introduces a potential vorticity method to answer this question.

It is encouraging that the ECMWF analyses can resolve the building of the downstream ridge by Opal. This is a process that has been previously documented by others (e.g., Wu and Emanuel 1995b; Bosart and Lackmann 1995). The constant generation of low potential vorticity air that builds the downstream ridge also maintains a 'phase lock' between Opal's latent heating maximum (associated with the cyclonic circulation) and the downstream ridge. This example of hurricane-environment interaction can also affect upstream features by retarding the approach of upstream shortwave troughs. Molinari et al. (1995) showed that Hurricane Elena's (1985) upper level EPV minimum, constantly reinforced by latent heating, compacted an approaching EPV maximum by resisting its associated shearing. This process occurred while Elena was still over warm water at a time when upper level outflow was well established. Molinari et al. (1995) noted that a tropical cyclone over cooler water (and similarly over land in the absence of an upstream trough that could provide support for regeneration) would lack the latent heating to resist upstream troughs. Opal at 1200 UTC 5 October was well inland and the upper level outflow was weakening with time. Over the last 12 h, however, convection and 'tropopause lifting' (Bosart and Lackmann 1995) by the outflow continued. As a consequence, Opal slowed (in a manner akin to the trough approaching Elena in 1985) the upstream shortwave trough by continuously building (and thus maintaining phase with) the downstream ridge.

Chapter 3

The Hurricane Steering Flow

This chapter places the idea of the hurricane steering flow into historical context. Section 3.1 introduces the concept of a hurricane steering flow. Section 3.2 reviews traditional (non-potential vorticity) methods of defining this flow. Section 3.3 describes observed systematic deviations from the defined flow, while section 3.4 gives the results of stratifying the data in order to explain the observed deviations. Section 3.5 introduces the potential vorticity method of defining the hurricane flow and its advantages.

3.1 The Idea of Hurricane Advection

The notion of a tropical cyclone being advected like a cork in a stream (Elsberry 1995) is an appealing analogy. That the storm, assumed to be a small (or point) cyclonic vortex, actually is steered by a large-scale environmental flow at its centre appears quite reasonable because there is a general poleward motion to hurricanes, with a westward component at low latitudes, then recurvature and an eastward component at higher latitudes. This motion is consistent with the tropical easterlies and the mid-latitude westerlies farther poleward. A relationship with the background state should be expected since hurricanes (neglecting upper level outflow) are, to a good approximation,

axisymmetric cyclonic vortices extending from the surface to the upper troposphere. They require no azimuthal variation of environmental parameters (e.g., baroclinicity) to exist since they draw their sustenance from fluxes of moisture from the ocean surface. Tropical cyclones are self-contained (i.e., isolated) in these respects.

For over 40 years, the idea of tropical cyclones being advected by the background flow has been extensively studied. The goal has been a simple definition of a steering flow from *observed* environmental flow fields, such as the observed or geostrophic winds. A simple, universally agreed upon, definition that minimizes statistical differences with the observed storm motion for many different storms has been elusive. It has been found that the steering flow concept can explain about 80 percent of the variability in 24-h forecasts of Atlantic storms (Wu and Emanuel 1995a).

3.2 Traditional Definitions of the Steering Flow

At the turn of the 20th century, forecasters realized that the movement of hurricanes was dependent upon environmental synoptic features. Bowie (1922) observed that the semi-permanent anticyclone in the western Atlantic steered hurricanes to the west. It was not until upper air data became available in the 1940s that a quantitative description of the steering flow was possible. For their description of the steering flow, Riehl and Burgner (1950) were restricted to the zonal flow in the lower troposphere (700 hPa and below) because of data availability and the coarse spacing of sounding stations. They expected, however, that the deep vertical structure of tropical cyclones made a *layer*, and not simply a *level* (such as their 700-hPa steering level, the level available to them that was most representative of the middle and upper tropospheric data), more likely to steer the storm. Horizontal spatial averaging was also required because of the remote chance of a sounding in the proximity of the storm centre.

Compositing of data to determine the best steering flow for a number of storms was also needed because of the scarcity of data for individual storms. Jordan (1952)

concluded that pressure-weighted averaged winds in an annulus from 2-4°-latitude radius from the storm centre best matched the observed motion. She also noted large deviations by individual storms and attributed these to a general oversimplification of the situation and to resolution problems of the steering flow.

Numerous studies since have defined stegring flows based upon observed winds or geostrophic winds calculated from the observed height field. Miller and Moore (1960) found both the 700 and 500-hPa levels to be optimum for predicting 24-h hurricane motion. George and Gray (1976) defined the steering flow to be a lower tropospheric 1-7° annular average. Chan and Gray (1982) claimed that the 5-7°-latitude radial band layer average from 500-700 hPa best matched cyclone motion.

There is general agreement that the lower and middle tropospheric flow over a near-storm domain best minimizes differences from the observed motion. However, individual storms can deviate significantly from these steering flows. Because of the variety of storm intensities and flow regimes, stratification of the data is needed to explain the systematic differences.

3.3 Systematic Deviations Identified by Flow Regime

Tropical cyclone-to-environment interaction contributes to the systematic deviations from observed motion. George and Gray (1976) showed that western North Pacific storms deviated to the left of the middle tropospheric flow. Chan and Gray (1982) found that movement was 10-20° to the left of the flow in the Northern Hemisphere but about 10° to the right in the Southern Hemisphere. Dong and Neumann (1986) concluded that, in the easterlies, storms moved to the right of the midtropospheric flow, but to the left in the westerlies, while Chan (1985) also found that westward moving storms tend to move to the right of the steering flow. The beta (i.e., the latitudinal variation of the Coriolis parameter, f) effect can explain propagation to the northwest of the position expected by steering alone (Chan and Williams 1987; Fiorino and Elsberry 1989; Franklin

et al. 1996). A potential vorticity explanation for the tendency for storms in the westerlies to drift to the left of their expected position has been given by Wu and Emanuel (1993). Their simple model showed that the upper level potential vorticity minimum of hurricanes can deflect the storms northward if it displaced downstream by upper level winds. This idea will be applied to Hurricane Opal in chapter 5.

3.4 The Effect of Storm Intensity on Steering Flow

Recent studies have further stratified data sets by storm intensity. Dong and Neumann (1986) calculated geostrophic flow from 20°-latitude finite differences of heights centred on the storm. The optimum steering levels were found to be 400 hPa for hurricanes and 700 hPa for tropical storms. The best steering layers in the easterlies were 1000-100 hPa (for hurricanes, i.e, sustained winds greater or equal to 33 m s^{-1}) and 1000-400 hPa (for tropical storms, i.e., sustained winds less than 33 m s^{-1}), and 1000-150 hPa (hurricanes) and 1000-300 hPa (tropical storms) in the westerlies.

Velden and Leslie (1991) used a barotropic model with various layer combinations of the observed environmental wind to advect a point vortex (the hurricane). The analyzed storms were necessarily removed by replacing the storms' circulations (extending to the outermost operationally-analyzed closed surface isobar) with a blend of the environmental wind field. The 700-hPa level, and 850-300-hPa and 850-400-hPa layers, minimized the 12-48-h forecast errors. The layer-*average* errors were consistently smaller in agreement with Dong and Neumann (1996) and Velden (1993). Velden and Leslie (1991) also stratified the 48-h forecast errors based on storm intensity (10-hPa intervals) using different layer means. Their results indicate that intense storms (< 955 hPa central pressure) are advected by a deeper layer mean flow from 850-300 hPa. For storms with central pressure > 975 hPa, the 850-500-hPa layer was optimum. Velden (1993) repeated the above procedure for Atlantic storms with similar conclusions. It has been theorized that the cyclonic cores of more intense storms extend farther into the upper troposphere

and so are steered by a deeper layer mean wind (Velden 1993). Merrill and Velden (1996) supported this theory by observing that the outflow of Supertyphoon Flo expanded to lower pressures during intensification.

Velden and Leslie (1991) noted that inclusion of the boundary and outflow layers (typically below 850 hPa and above 300 hPa) may prove disadvantageous to the definition of the steering flow.

3.5 The Potential Vorticity Definition of the Steering Flow

Potential vorticity descriptions of tropical cyclones have focussed on storm structure (Shapiro and Franklin 1995; Merrill and Velden 1996), intensity (Molinari et al. 1995; Bosart and Lackmann 1995) and motion resulting from hurricane-to-environment interaction (Wu and Emanuel 1993, 1994; Wu and Kurihara 1996).

This work applies potential vorticity to the hurricane advection problem. Its flexibility provides a powerful and physically revealing method, only now being explored in the literature, to retrieve the environmental steering flow. The invertibility principle is exploited to remove the primary cyclonic circulation of Hurricane Opal and recover the remaining synoptic environment. This general technique has been used by Wu and Emanuel (1995a,b) in their two-paper EPV retrieval of the steering flows for Tropical Storm Ana and Hurricanes Bob and Andrew. As well, Shapiro (1996) applied an inversion to the extensive dataset of Hurricane Gloria. The method used in the current work builds upon the removal by Wu and Emanuel (1995a) of the storm circulation from the potential vorticity anomaly (with respect to a suitably defined climatology) field and boundary conditions. (Details of past studies and the present method, including inversion, are given in chapter 4). Once the environmental flow has been retrieved, a steering flow is obtained based on the idea that storm motion results from deep-layer environmental advection of the low and mid-level local potential vorticity maximum of Opal associated

with the cyclonic circulation of the storm. This horizontal averaging is more physically-based than seen in earlier potential vorticity studies.

There are three major advantages of potential vorticity methods over traditional methods. First, the intensity and fine-scale structure of mesoscale hurricanes is poorly resolved using traditional synoptic-scale analyses. We thus remove the poorly represented hurricane from the synoptically-based QGPV fields leaving the much better represented QGPV field of the environment to determine the storm's motion. [Incidentally, QGPV also cannot capture well the features of a mesoscale hurricane; see section 4.2]. The flow over the storm's position associated with the remaining potential vorticity distribution then defines the steering flow. In this way, the ability of the data analysis procedure to well represent the storm's circulation is less important, in contrast to traditional methods. Second, the domain for horizontal averaging of the wind field becomes much more easily defined. Instead of a subjective annular or radial averaging procedure based on an ideal composite storm, the wind field is averaged over the domain of the storm's localized potential vorticity anomaly. Indeed, it is this feature, responsible for the cyclonic circulation of the storm, that is being advected. As well, the averaged wind is much less sensitive to the choice of domain when the storm has been removed due to the relatively weak gradients of the background synoptic flow. Third, and most attractive of all, the quantitative contribution to the steering flow by different synoptic features can be determined from the piecewise inversion property. This principle has great implications for the verification of numerical forecasts (Davis and Emanuel 1991). The use of potential vorticity makes it possible to determine the specific synoptic feature(s) misrepresented by a model in a poor forecast. This study attempts to determine the specific synoptic feature(s) improperly simulated by the United States' operational short-range eta forecast model.

Chapter 4

QGPV and Inversion Methodology

This chapter defines quasi-geostrophic potential vorticity and inversion techniques. The conditions for the use of QGPV for tropical systems are shown to be met. The inversion procedure is then detailed and compared and contrasted against established inversion methods in the literature. The post-inversion procedure for computing the steering flow is given.

4.1 Quasi-Geostrophic Potential Vorticity

To take advantage of the benefits of potential vorticity methods, we use QGPV (Charney and Stern 1962), defined on an f-plane in isobaric coordinates as

$$q = \frac{1}{f_o}\nabla^2 \phi' + f + f_o \frac{\partial}{\partial p}\left(\frac{1}{\sigma_r}\frac{\partial \phi'}{\partial p}\right), \qquad (4.1)$$

where ∇^2 is the two-dimensional Laplacian operator in pressure coordinates, ϕ' the geopotential anomaly from an isobarically-averaged reference atmosphere (here taken to be the U.S. Standard Atmosphere), f the Coriolis parameter and $f_o = 10^{-4}$ s^{-1}. The static stability coefficient is

$$\sigma_r = - \frac{\alpha}{\theta} \frac{d\theta_r}{dp} , \qquad (4.2)$$

where θ_r is the potential temperature of the reference atmosphere and α the specific volume. Note that the units of QGPV (s^{-1}) are the same as vorticity.

The geostrophic relative vorticity is

$$\zeta_g = \frac{1}{f} \nabla^2 \phi' , \qquad (4.3)$$

which can be derived from the zonal and meridional geostrophic wind components

$$u_g = - \frac{1}{f_o} \frac{\partial \phi'}{\partial y}; \quad v_g = \frac{1}{f_o} \frac{\partial \phi'}{\partial x} . \qquad (4.4)$$

Then (4.1) can be rewritten as

$$q = [\zeta_g + f] + f_o \frac{\partial}{\partial p} \left(\frac{\theta'}{d\theta_r / dp} \right) . \qquad (4.5)$$

In this form, QGPV is seen to be composed of two general terms. The first term on the RHS of (4.5) is the geostrophic absolute vorticity (the sum of geostrophic relative vorticity and planetary vorticity) while the second is related to the static stability. QGPV is conserved following horizontal geostrophic air motion in the absence of friction and diabatic heating effects.

4.2 The Concept of (QG) Potential Vorticity Inversion

An attractive feature of potential vorticity is the ability to retrieve all atmospheric dynamic and thermodynamic variables through a procedure called inversion. With knowledge of the atmosphere's three-dimensional potential vorticity structure, appropriate

boundary conditions and a balance relationship between the height field (Φ) and streamfunction (Ψ) (and wind field), the original state of the atmosphere can be retrieved.

Rewriting (4.1) as a linear, elliptic, differential operator $\mathcal{L}$ acting upon the anomalous geopotential field ϕ' (after HMR), gives

$$\mathcal{L}\,[\phi'] = q_* = [\frac{1}{f_o}\nabla^2 + f_o\frac{\partial}{\partial}\,(\frac{1}{\sigma_r}\frac{\partial}{\partial p})]\;\phi' \;, \qquad (4.6)$$

where $q_* \equiv q - q_r$ and $q_r = f$, the value of QGPV in the U.S. Standard Atmosphere. Thus, the operator acting upon the geopotential anomaly is equal to the QGPV anomaly (both with respect to the reference atmosphere). In general, q_* can be arbitrarily partitioned, such that

$$q_* = \sum_{i=1}^{n} q_{*i} \;. \qquad (4.7)$$

The process of piecewise inversion refers to the retrieval of the anomalous geopotential fields ϕ_i', associated with each q_{*_i}, through inversion of the operator $\mathcal{L}$. That is,

$$\phi_i' = \mathcal{L}^{-1}\,(q_{*i}) \;, \qquad (4.8)$$

such that

$$\phi' = \sum_{i=1}^{n} \phi_i' \;. \qquad (4.9)$$

The hydrostatic equation, geostrophic wind relations and QG omega equation can then be applied to the retrieved geopotential anomalies to compute, respectively, the temperature field and horizontal and vertical velocity fields. Thus dynamical and thermodynamical variables associated with *distinct* parts of the observed potential vorticity distribution can be obtained through piecewise inversion.

The linearity of the QG balance equation (appropriate when using QGPV) guarantees the retrieval of *unique*, independent geopotential components, said to be

'induced' by each q_{*i} distribution, whose sum equals the total original anomalous geopotential field ϕ'. This fact makes QGPV much cleaner and simpler than EPV inversion, which requires that a non-linear balance equation, most often that of Charney (1955), be linearized. EPV inversion in this manner has been carried out by Davis and Emanuel (1991) and Davis (1992a,b). Non-hurricane QGPV studies include Robinson (1988), Holopainen and Kaurola (1991), Black and Dole (1993) and Hakim et al. (1995, 1996).

Use of the QG system and QGPV is justified for synoptic- (or larger) scale flows in which the Rossby number,

$$R_o = \frac{U}{\Omega L}, \qquad (4.10)$$

where U ~ 10 m s^{-1} is a typical horizontal flow speed, $\Omega = 7.292 \times 10^{-5}$ s^{-1} the angular rotation rate of the earth and L ~ 10^6 m a typical horizontal scale, is negligible. For this reason, QGPV is unsuitable to describe the mesoscale details of tropical features such as hurricanes. Davis (1992a) states that the relative vorticity in the inverted flow must be two or three times the Coriolis parameter for distortions to appear in the position of QGPV anomalies compared to the more accurately defined EPV anomalies. This situation is only of concern for the QGPV anomaly of Opal itself, which is ultimately removed. We strive to determine the steering flow of Hurricane Opal associated with synoptic-scale potential vorticity anomalies. Hakim et al. (1996) showed that their synoptic scale fields of QGPV and EPV had a high correlation factor of approximately 0.85. It will be shown that the steering flow is associated with synoptic-scale extratropical features that permit the use of QGPV.

4.3 QGPV Inversion Method

4.3.1 Method for ECMWF Analyses

The following procedure was first performed on ECMWF analyses (described in section 2.2.2). QGPV fields from 950 hPa to 150 hPa, every 50 hPa, were calculated for analyses valid at 0000 UTC 4 October and 0000 UTC and 1200 UTC 5 October 1995. The domain of integration is shown in Fig. 4.1.

a) The Positive Storm Anomaly and Partitioning Strategy

Quantitative identification of Opal's interior positive QGPV anomaly ('positive storm anomaly', hereafter PSA) at each pressure level was accomplished by defining a climatological background QGPV field computed from 10 years of October geopotential heights (Trenberth 1992). The QGPV anomaly field was defined as the observed field minus the climatological field.

The reasons for this primary partitioning strategy are two-fold. First, the PSA is now identifiable as a compact strongly positive lower and middle-tropospheric anomaly (Figure 4.2 is a representative example of the anomalous QGPV field). However, because of the proximity of adjacent anomalies not directly associated with the axisymmetric storm core (due possibly to earlier latent heating events), the exact choice of grid points that defined the PSA was subjective. The periphery of the PSA was not always axi-symmetric and was often irregularly shaped. We thus allowed our PSA to be irregularly shaped, in contrast to Wu and Emanuel (1995a), within reason. Several test inversions designed to elicit the sensitivity to small changes in the number of PSA grid points (of which there were 30-50 at each level) indicated that the effects on the retrieved fields were small, as seen by Wu and Emanuel (1995a). The above definition of the PSA

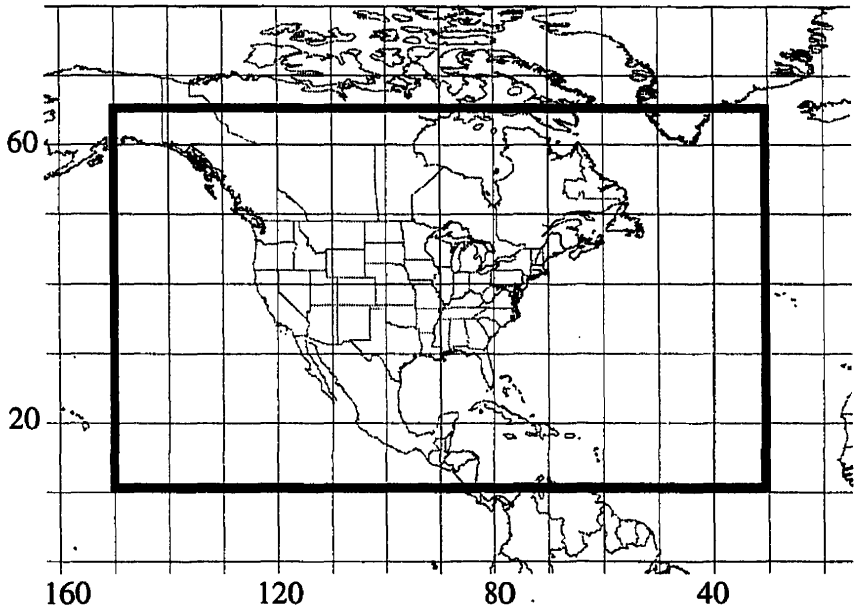

Fig. 4.1. Domain used for ECMWF QGPV inversions. The region is a rectangle with lower left and upper right coordinates 10° N 150° W and 65° N 30° W, respectively.

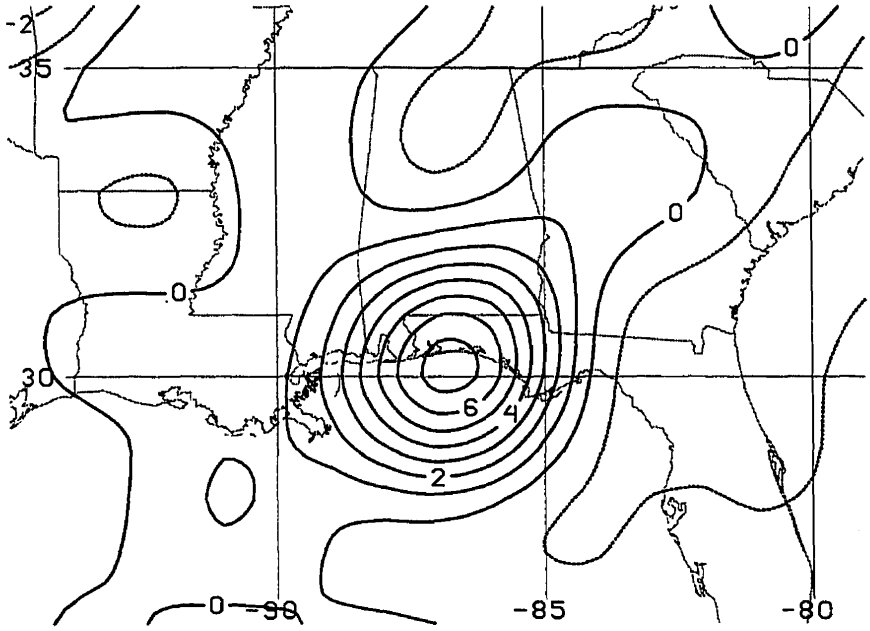

Fig. 4.2. Anomalous QGPV field with the PSA included (units are 10^4 s^{-1}, contoured every 10^4 s^{-1}) at 0000 UTC 5 October.

effectively removes, by making small, any undesired self-advection by non-axisymmetric latent heating effects (i.e., the irregularly shaped PSA, as noted by Wu and Emanuel 1995a) from our results. We allow any anomalous positive QGPV up to 150 hPa to be part of the PSA since strong storms exhibit deeper circulations and Opal was within a region devoid of upper-level cyclonic potential vorticity anomalies. Wu and Emanuel (1995a) defined their tropical cyclones' EPV anomalies (their LS) at, and below, 300 hPa.

Second, anomalous synoptic-scale flow with respect to a largely zonal (near Opal) climatology can be identified. The anomalously low geopotential (not shown) over the Gulf of Mexico in early October was left as part of the anomaly field. This partitioning allows wind fields to be associated with either general potential vorticity gradients (the zonal climatological flow) or isolated anomalies (synoptic features responsible for meridional flow).

To evaluate the contribution to the steering flow by the earlier-identified synoptic-scale ridge and trough, we further partitioned the anomalous QGPV field into cyclonic (positive) and anticyclonic (negative) anomalies, following Lackmann and Gyakum (1996) and Lackmann et al. (1997). This partitioning strategy allows for direct hurricane-to-environment effects (and the model's representation) to be retained in the inversions in the form of the hurricane's upper-level negative anomaly.

b) Removal of the PSA

The PSA of Hurricane Opal was extracted (i.e., arithmetically cut-out) at each interior level (950-150 hPa) from the anomalous QGPV field by replacing grid points within the PSA with the climatological QGPV value (i.e., an anomaly of magnitude zero). The resulting anomaly field was then partitioned into three component fields, hereafter designated as ANOM (positive plus negative anomalies, minus the PSA), CYCLO (positive anomalies, minus the PSA) and ANTI (negative anomalies).

The replacement of the PSA of a tropical system by a zero-anomaly follows Wu

and Emanuel (1995a). Hakim et al. (1996) also replaced the domains of the precursors of the 'Cleveland superbomb' (defined by Hakim et al. (1995) as the vertical cylinder encompassing the last closed contour, at 0.5-PVU intervals, of 500-hPa QGPV) with a zero-anomaly in order to obtain the background flow.

c) Boundary Conditions

The inversion of the differential operator requires lateral and horizontal boundary conditions (BC). Typically either perturbation geopotential (Dirichlet-type) or perturbation potential temperature (equivalently, through the hydrostatic relation, the normal derivative of perturbation geopotential) (Neumann-type) is specified.

The traditional horizontal BC, given by HMR, is homogeneous Neumann (i.e., zero potential temperature anomaly), while Davis and Emanuel (1991), Davis (1992a), Bresky and Colucci (1996), Wu and Emanuel (1995a,b) use inhomogeneous Neumann (observed potential temperature anomaly). We specify (zero and non-zero, in succession; see below) Dirichlet BCs after Hakim et al. (1996). They used homogeneous Dirichlet BCs (still an arbitrary choice) and found that their QGPV inversions suffered less cancellation than with Neumann BCs when required to yield the analyzed horizontal boundary perturbation geopotential fields. Their results were also less sensitive to tests involving changes in the Dirichlet BCs than for the Neumann-type.

As is the case with most piecewise potential vorticity inversions, defining the appropriate lateral BCs is difficult because the contribution from each partitioned interior anomaly to the observed value on the boundary is impossible to know *a priori*. This problem is usually minimized by inverting over the entire hemisphere (which is often too computationally expensive) or by selecting a domain of integration to extend at least one Rossby radius beyond the region of interest (Davis 1992a). In the latter case, the boundaries have little influence and can simply be made homogeneous Dirichlet (Davis and Emanuel 1991; Wu and Emanuel 1995a; Hakim et al. 1996).

Specification of the lower BC is also problematic because the goal of removing the entire storm cyclonic circulation is not accomplished by simply removing the PSA. Wu and Emanuel (1995a) simply define the hurricane advection flow to be the entire potential vorticity distribution and BCs, excluding the PSA itself and the positive lower boundary potential temperature anomaly over the same domain. Thus their lower BC for the environmental flow contains all lower boundary theta anomalies, except the positive anomaly in the vicinity of the storm. We attempt to quantify, then remove from the lower BC, the negative geopotential anomalies (analogous to positive theta anomalies) associated with the PSA and associated with the surface potential temperature anomaly (hereafter, the latter will be called the 'secondary' effects).

It should be noted that, because of the Laplacian in the operator in (4.6), the effects we desire to remove extend horizontally over an area much greater than that of the PSA. The observed lower theta anomaly (that contributes to an area of depressed geopotential when using Dirichlet BCs) is not necessarily representative of the extent of the influence of the PSA on the lower BC. [Regions exterior to the local negative geopotential anomaly may be influenced by Opal but still have an overall positive geopotential anomaly because of stronger influences by synoptic features]. In this case, the observed geopotential was lower everywhere in the southeastern U.S. and Gulf of Mexico and so it would be unrealistic to attribute the entire negative anomaly in the region to Opal (as done by Wu and Emanuel (1995a) for their storms, i.e, they removed the PSA and lower boundary anomaly from the same domain).

For the same reason, we choose not to follow Hakim et al. (1996) who inverted the domains of their precursors with homogeneous Dirichlet BC and then, to retrieve the environmental flow, subtracted the resulting geopotential anomalies from the total observed field. We remove the secondary effects on the lower boundary by using the appropriately-scaled inverted anomalous geopotential field induced by the PSA to restore the lower boundary anomalous geopotential field to an environmental (but not climatological) value.

The secondary effects take the form of a quasi-axisymmetric 'cone' of anomalous geopotential with a negative central value that decreases to negligible values at large

radial distances. Again, we desire to preserve the synoptic-scale gradients in the vicinity of Opal that help steer the storm. To do this we must obtain a cone whose structure is based largely on observations. We thus invert the PSA with homogeneous Dirichlet lateral and horizontal BC to obtain the induced three-dimensional anomalous geopotential field. The induced 700-hPa (Fig. 4.3a) and vertical (Fig. 4.3b) structure at 0000 UTC 5 October, which is representative of all times, is almost axisymmetric as expected. Because of the imposed BC, however, the magnitude decreases vertically towards the horizontal BC and is exactly zero on the lower boundary. This, however, is the level at which we desire the induced ϕ' which prevents this field from simply being subtracted from the observed field.

To overcome this, we use the inverted ϕ' field of the PSA at 700-hPa as a proxy for the value on the lower boundary. This level is assumed to be close enough to the lower boundary to be representative. We now have a cone of ϕ' representative of the effects of the PSA on the lower boundary but whose magnitude has been diminished by the imposed homogeneous BC. The entire 700-hPa ϕ' field is then multiplied by a scalar to correct for the effects of the imposed homogeneous lower BC.

The scalar factor that increases the magnitude of the 'cone' and, as a beneficial side-effect, mathematically incorporates other secondary effects mentioned above (e.g., the effect of the lower potential temperature anomaly of the storm).

We define a constant background (really 'environmental' but called the 'background' since 'environmental' is already in use) state by invoking a modified version of the Radius of the Outer Closed Isobar (ROCI) method (Merrill 1984; Velden and Leslie 1991). The value of ϕ' at the radius of the largest closed isobar (analyzed at a 1-hPa interval) at eight compass points (the four cardinal plus the intermediate directions) at 0000 UTC, 0600 UTC and 1200 UTC 4 October was obtained and the results averaged (refer to Table 4.1). This defined the background value of ϕ' in the vicinity of Opal, assumed to be constant in time and space over the period of study (0000 UTC 4 October to 1200 UTC 5 October).

The anomalous geopotential values obtained by the ROCI procedure at times later

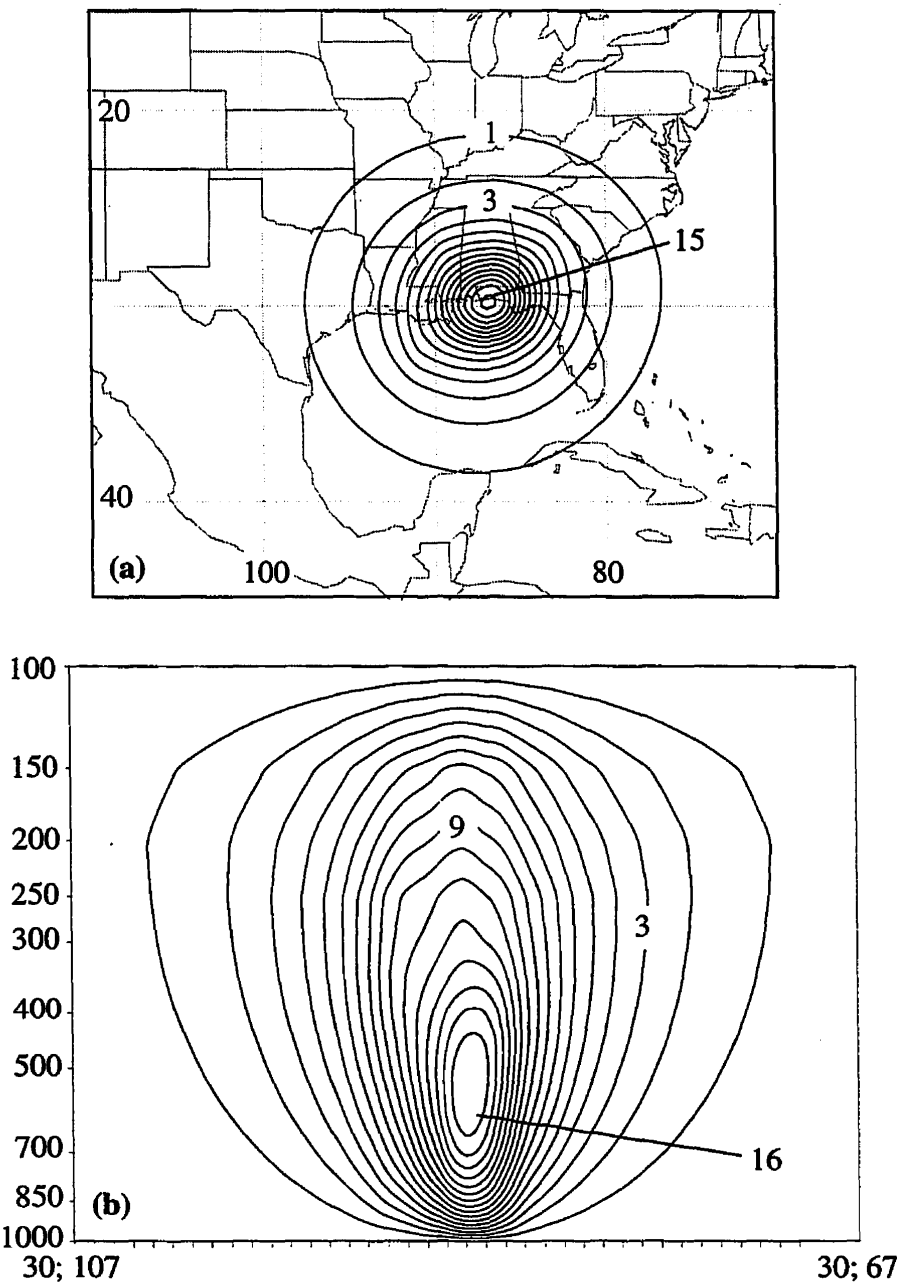

Fig. 4.3. Anomalous geopotential field induced by PSA for 0000 UTC 5 October: (a) at 700 hPa and (b) vertical cross-section east-west through the centre of Opal along 30° N from 107° to 67° W. Units are 10^{-2} m^2 s^{-2}.

Table 4.1

Model	Time/Date (hour/day)	ROCI ϕ' Average
ECMWF	0000/4	-7.11
ECMWF	0600/4	-5.68
ECMWF	1200/4	-6.54
ECMWF	1800/4	-8.12
ECMWF	0000/5	-13.7
ETA	0000/4	-11.20
ETA	1200/4	-10.62
ETA	0000/5	-15.23

Observed geopotential anomalies (10^{-2} m^2 s^{-2}) obtained from the ROCI method on the lower boundary.

than 1200 UTC 4 October were affected by the approaching extratropical cyclone to the northwest. The western low's circulation encroached upon that of Opal and reduced the number of closed isobars surrounding the storm, even when Opal's intensity remained relatively constant in the models analyses. The ROCI was severely reduced to the west through north of Opal and so the observed ϕ' were much more negative than at earlier times (Table 4.1) and unrepresentative of values at the periphery of Opal's unobstructed circulation. As a result, they were not included in the ROCI averages.

The central (most negative) 1000-hPa ϕ' background value is next subtracted from the observed central 1000-hPa value, then divided by the central value of the 700-hPa field. The scale factor is thus

$$\iota = \frac{\phi'_{ob} - \phi'_{bg}}{\phi'_{inv}} , \qquad (4.11)$$

where ϕ'_{ob} is the observed, ϕ'_{bg} the background and ϕ'_{inv} the inverted, field, respectively. Table 4.2 gives the relevant values of ϕ', including the computed scale factors. The scaled-700-hPa field is then subtracted from the observed 1000-hPa field to obtain the lower boundary condition. Figure 4.4a shows the observed lower boundary field at 0000 UTC 5 October (representative of other times) while Fig. 4.4b shows the lower BC with Opal's effects removed (hereafter, the 'adjusted' BC). This adjusted lower BC shows that a significant portion of Opal's circulation has been removed following the systematic procedure that is detailed above and summarized in Table 4.3. The difference between Figs. 4.4a and 4.4b (not shown) is a very good representation of the cyclonic component of Opal on the lower boundary.

The observed anomalous geopotential was used as the ANOM upper BC because the PSA is largely a low and mid-tropospheric feature and so the cyclonic effects at 100 hPa were much weaker than at 1000 hPa. As well, the negative anomaly (outflow) at upper levels was left in the inversions. The observed geopotential anomaly field was used as the lateral BC since the inversion boundaries were sufficiently distant.

The CYCLO (ANTI) inversions used the adjusted lower BC for regions with

Table 4.2

Model	Time/Date/ Forecast hour	1000-hpa observed	1000-hPa background	700-hPa inverted	ι
ECMWF	0000/4/F00	-26.09	-6.44	-12.66	1.55
ECMWF	1200/5/F00	-27.55	-6.44	-12.32	1.71
ETA	1200/5/F00	-29.40	-10.91	-14.59	1.27
ETA	0000/5/F12	-22.75	-10.91	-7.93	1.49
ETA	1200/3/F48	-26.16	-10.91	-10.29	1.48

Values of anomalous geopotential (10^{-2} m^2 s^{-2}) and scale factor associated with determination of the lower boundary condition using the ROCI method. Data are given for different model runs and valid times.

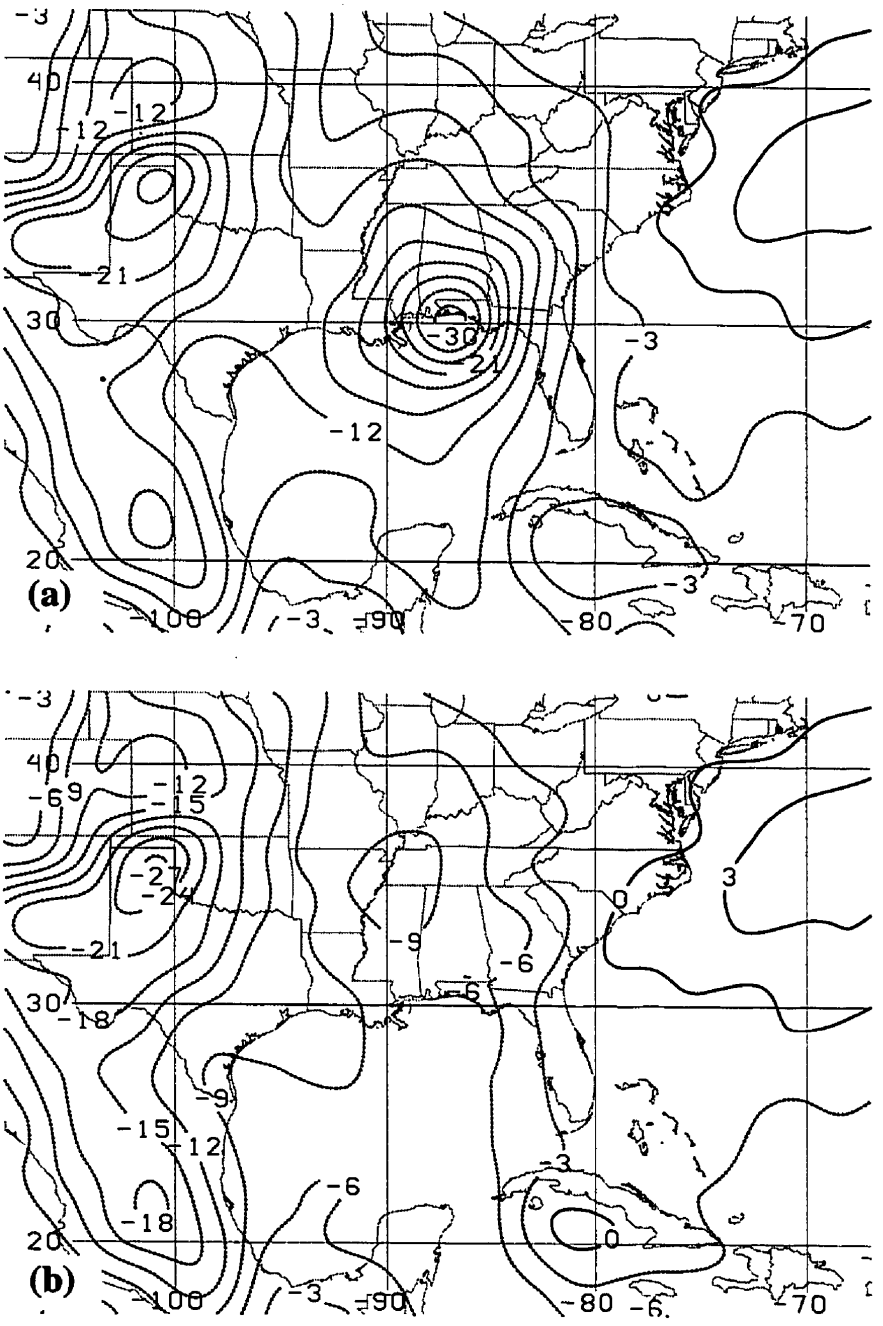

Fig. 4.4. Lower boundary field of anomalous geopotential for 0000 UTC 5 October: (a) observed and (b) adjusted. The units are 10^{-2} m^2 s^{-2}, contoured every $3x10^{-2}$ m^2 s^{-2}.

Table 4.3

The following inversion procedure was carried out for each time (except 4b which was calculated once only for the ECMWF and the eta data):

1. Identify Opal's interior positive QGPV anomaly with respect to climatology (the PSA)
2. Remove the PSA
3. Partition ANOM (positive and negative, minus PSA) into CYCLO (positive minus PSA) and ANTI (negative)
4. Specification of BC:
   - remove secondary effects from lower BC:
   a) invert PSA with homogeneous horizontal and lateral Dirichlet BC
   b) compute background field around Opal using the ROCI procedure
   c) calculate scale factor (using (4.11))
   d) scale the 700-hPa inverted anomalous geopotential field
   e) subtract the scaled 700-hPa field from the observed 1000-hPa anomalous geopotential field to obtain the 'adjusted' Dirichlet lower BC for ANOM
   f) use adjusted ANOM lower BC, with regions of positive anomaly made zero, as Dirichlet lower BC for CYCLO
   g) use adjusted ANOM lower BC, with regions of negative anomaly made zero, as Dirichlet lower BC for ANTI

   - use observed anomalous geopotential (Dirichlet-type) at 100-hPa for ANOM upper BC; use the same (with positive areas made zero) for the CYCLO upper BC and the observed (with negative areas made zero) for the ANTI upper BC

   - for the lateral BCs, do as for the upper horizontal BC

Summary of procedure followed for inversions of ECMWF and eta data.

negative (positive) anomalous geopotential and a homogenous BC for regions with positive (negative) anomalous geopotential. These conditions were used because positive (negative) QGPV and potential temperature anomalies can only induce negative (positive) geopotential anomalies. The lateral BCs were similarly partitioned.

d) The ECMWF Inversions

Static inversions were numerically performed (using an under-relaxed method out to 2000 iterations) on analyses valid at 0000 UTC 4 October and 0000 UTC and 1200 UTC 5 October for the three partitioning strategies ANOM, CYCLO and ANTI.

4.3.2 Method for Eta Inversions

The procedure outlined in section 4.3.1 was next performed on eta model forecasts and analyses. QGPV fields from 950 hPa to 150 hPa, every 50 hPa, were calculated for analyses valid at 1200 UTC 4 October and 0000 UTC and 1200 UTC 5 October 1995. Eta model forecasts of 24 h valid at 1200 UTC 4 October, of 12, 24 and 36 h valid at 0000 UTC 5 October and of 12, 24, 36 and 48 h valid at 1200 UTC 5 October, were inverted. Eta data were available on a one-standard parallel (25°N) Lambert conformal projection with an 80 km resolution at 25° N. The inversion domain for the eta model is shown in Fig. 4.5.

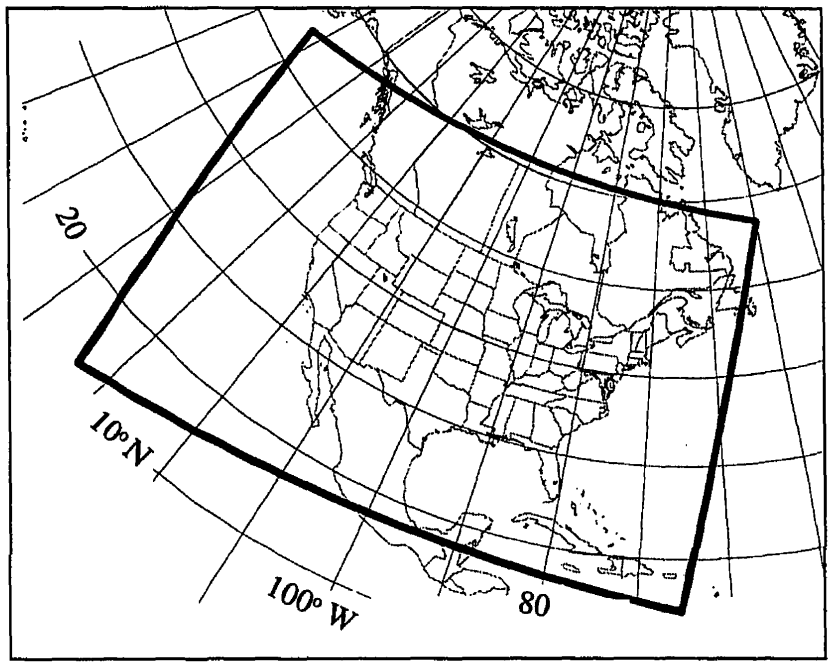

Fig. 4.5. Domain used for eta QGPV inversions. The bottom left and upper right coordinates are 12.19° N 133.46° W and 57.29° N 49.38° W, respectively.

Chapter 5

Results - The Deep-Layer Steering Flow

5.1 Computation of the Deep-Layer Geostrophic Wind Field

The f-plane anomalous geostrophic winds were computed every 50 hPa from 950 to 150 hPa for ANOM, CYCLO, ANTI, climatology (hereafter, CLIMO) and FULL (sum of ANOM and CLIMO). Following Velden and Leslie (1991) and Velden (1993), the components of these winds were vertically averaged from 850 to 300 hPa to obtain the deep-layer steering flow. Figure 5.1 shows that the contribution by CLIMO is largely zonal and increases to the north in the westerlies.

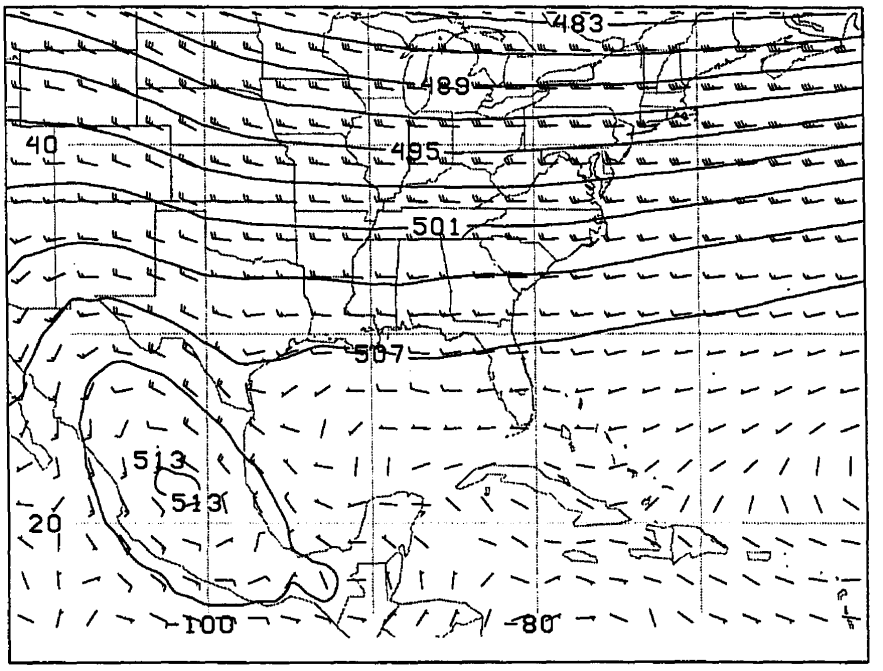

Fig. 5.1. The CLIMO deep-layer (850-300 hPa) average geopotential height (dam). Contour interval is 3 dam.

5.2 Inversion Results

5.2.1 ECMWF and Eta Analyses

a) Horizontal Geopotential and Wind Fields

The FULL ECMWF analysis at 0000 UTC 4 October (Fig. 5.2a) places Opal in a disorganized but overall southerly steering flow consistent with the observed south-southwesterly motion (Table 2.1). Distinct circulation centres of a northeast-southwest oriented ridge are located just off the U.S. east coast (deep-layer average geopotential above 516 dam) and in the Gulf of Mexico (above 513 dam). The western low's effects (Fig. 5.2b) are small. However, the southerly winds ahead of a trough over the Mississippi river valley may be enhancing the southerly flow over the Gulf of Mexico and Gulf states. Low-level potential vorticity anomalies associated with earlier precipitation (see Figs. 2.2 through 2.4) may be responsible for this stronger flow. The ANTI contribution, appearing as an elongated region of anomalously high geopotential (Fig. 5.2c), has one closed centre south of New England (above 21 dam) and another to the northeast of Opal (above 18 dam). The overall pattern of an eastern ridge prevents Opal from having a significant easterly motion.

The remainder of this study focusses on 1200 UTC 5 October (consistent with results of 0000 UTC 5 October, not shown) when the steering flow was especially robust.

The ECMWF analysis at 1200 UTC 5 October (Fig. 5.3a) shows a more extensive and significant southerly flow from Florida to Texas. The eastern ridge has built above 522 dam and consolidated into one northeast-southwest oriented cell just off the U.S.' southeast coast. The geopotential gradient (and steering flow) has increased in response to movement of the now well-defined western low eastward into central Nebraska and building of the eastern ridge. The CYCLO circulation in Fig. 5.3b over southeastern Nebraska now contributes a strong northward flow component over Opal. [Note that the position of the vertically-averaged baroclinic (tilted) disturbance need not necessarily

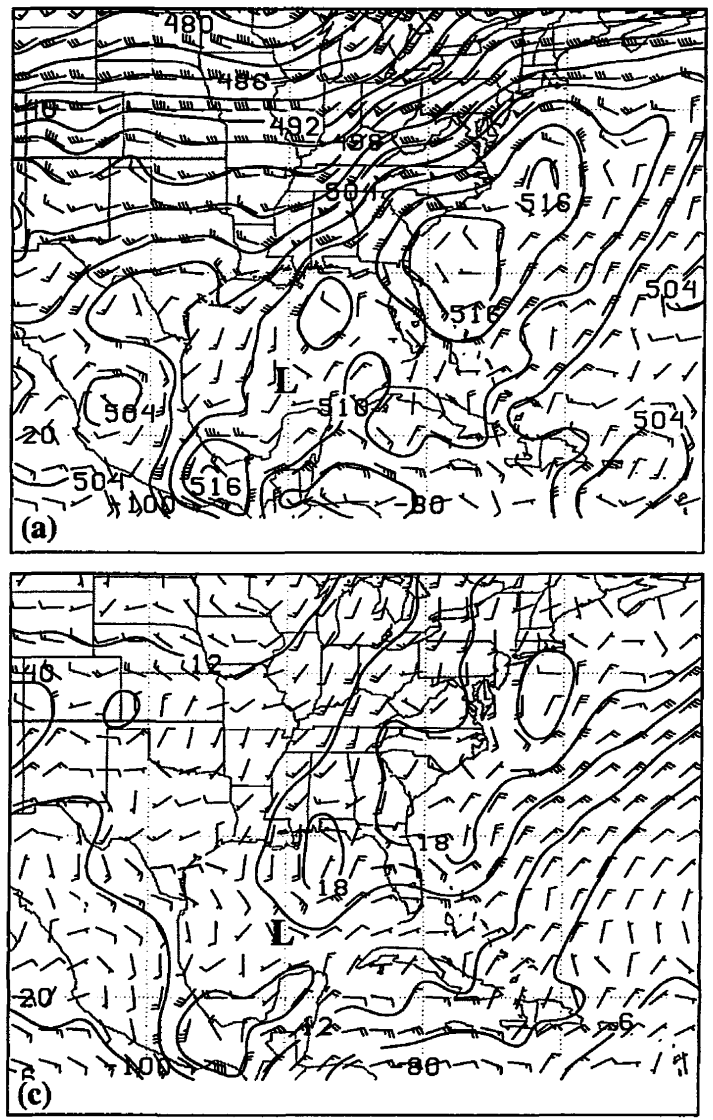

Fig. 5.2. Deep-layer steering flow and geostrophic winds, valid at 0000 UTC 4 October, for the ECMWF analysis. Panel (a) is the FULL geopotential heights (sum of Figs. 5.1, 5.2b and 5.2c). Panels (b) and (c) are the CYCLO and ANTI-induced anomalous geopotential heights (in dam), respectively. Contour interval is 3 dam. Position of Opal is denoted by the 'L'.

Fig. 5.3. As in Fig. 5.2, except valid at 1200 UTC 5 October. Opal is denoted by the 'L' over northeastern Alabama.

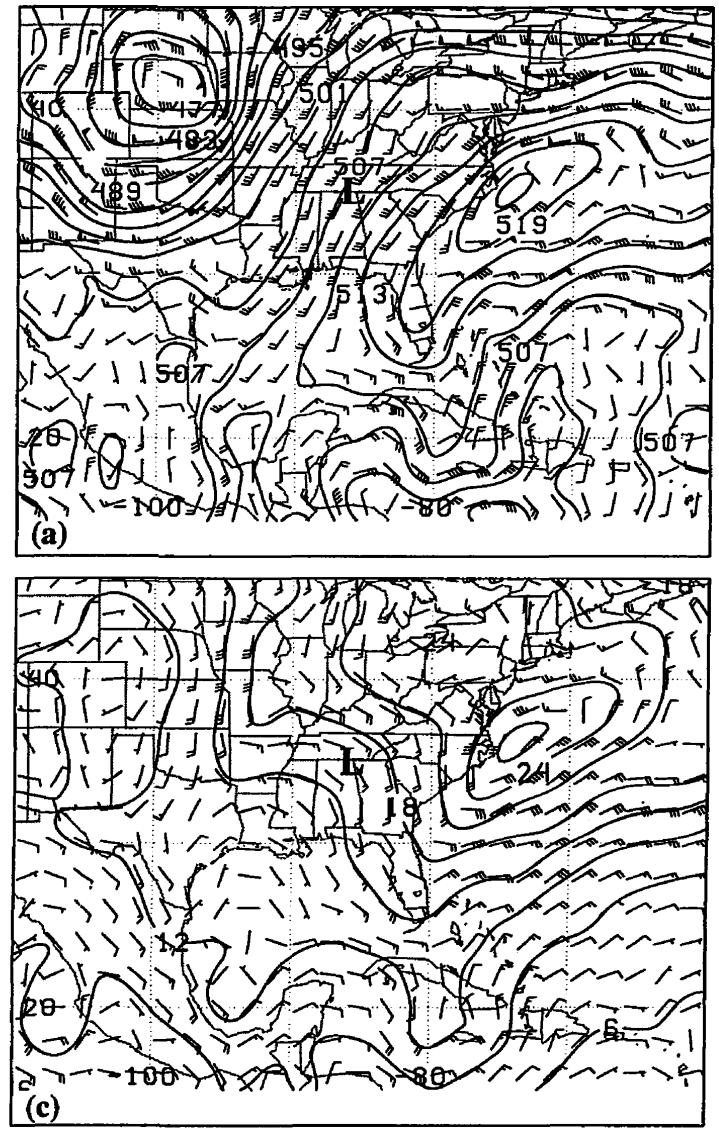

correspond to the location of lowest surface pressure]. Of note is the warm frontal trough extending eastward to Tennessee (Fig. 5.3b). This feature is largely obscured in the FULL field (Fig. 5.3a) by the circulation of the extension of the eastern ridge over Missouri (Fig. 5.3c). Meanwhile, the circulation of the upper low east of the Bahamas (Fig. 5.3b) is enhancing the northeasterly flow in the western Atlantic around the eastern ridge. Figure 5.3c shows that ANTI has consolidated and strongly built the ridge to above 27 dam off the mid-Atlantic coast. The expansion of the ridge over, and south, of the Great Lakes (anomalous geopotentials have risen up to 8 dam) strongly contributes to Opal's increased forward speed with the storm being steered by ANTI to the northwest.

In comparison, the FULL eta analysis (Fig. 5.4a) significantly under-represents the eastern ridge compared to the ECMWF, with the deep-layer geopotential maximum of about 513 dam farther south along the southeast U.S. coast and in the western Atlantic. The western low (Fig. 5.4b) is similarly positioned, however, the eastern upper low evident in Fig. 5.3b appears only as a broad trough extending from the western low. The eta model's ANTI (Fig. 5.4c) is weaker with a smaller geopotential gradient on its western periphery because the strong closed cell off the mid-Atlantic states is not present. Note, however, the closed cell above 24 dam in eastern Ohio immediately northeast of Opal.

Both analyses at 1200 UTC 5 October generally resolve strong ANTI-induced ridging from the mid-Atlantic coast to the Great Lakes downstream (with respect to the upper flow) of Hurricane Opal. The ECMWF's robustness is attributed to substantially lower QGPV along the U.S. east coast that is uniquely capable of raising heights.

b) Vector Wind Fields

The horizontal wind fields were then horizontally averaged over the domain of the PSA for CLIMO, CYCLO, ANTI, ANOM, FULL and TRAD, a traditional average of the observed height fields over a 5-7° annulus. The components are plotted as vectors, in a manner similar to the hodographs of Wu and Emanuel (1995a,b), along with the observed

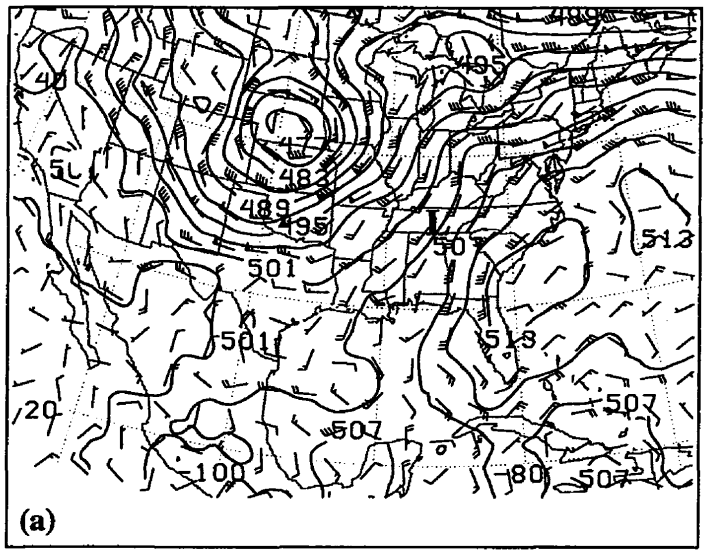

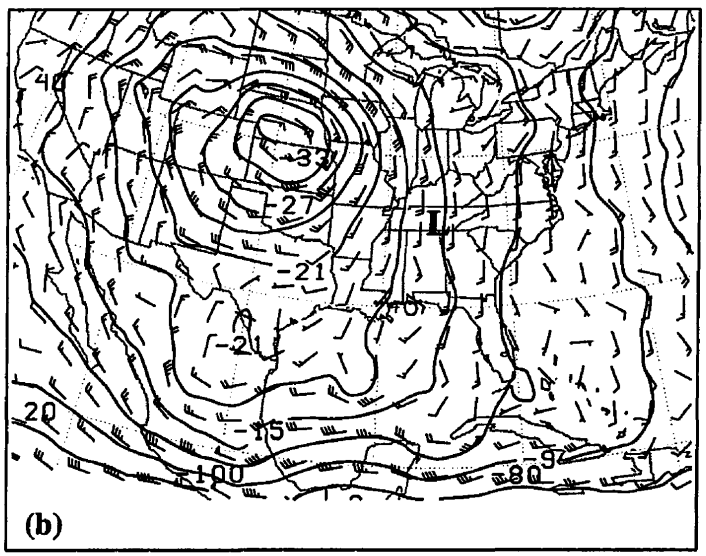

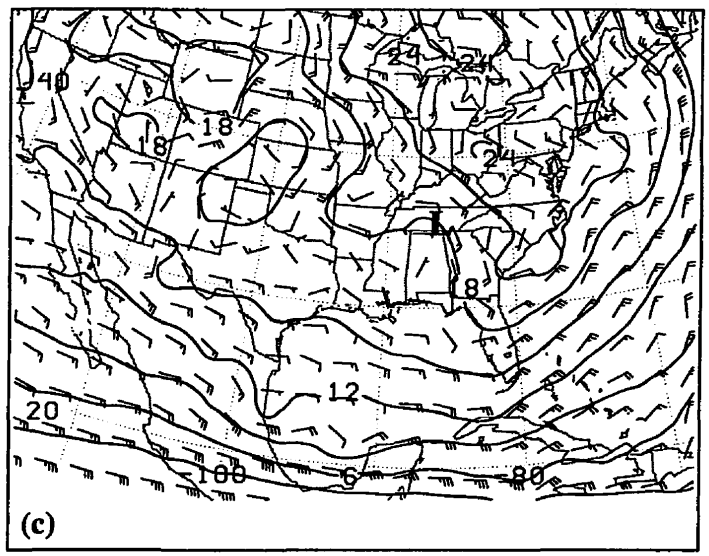

Fig. 5.4. As in Fig. 5.2, except for eta analysis valid at 1200 UTC 5 October. Opal is denoted by the 'L' over Tennessee.

storm motion (OBS).

The FULL inverted winds from the ECMWF analysis at 0000 UTC 4 October (Fig. 5.5a) accounts for 54% of the observed storm motion of 7.2 m s^{-1}. Of this, 23% is from CYCLO and 15% by ANTI, with a CYCLO to ANTI ratio of 1.6. Refer to Table 5.1 for a summary.

At 1200 UTC 5 October (Fig. 5.5b), the ECMWF FULL vector accounts for a large part (89%) of OBS, with a substantial contribution from ANTI (19%). CLIMO has increased from Fig. 5.5a because of the analyzed position farther north in the westerlies. The eta analysis at the same time (Fig. 5.5c) is encouragingly similar, lending credence to the inversion procedure. In fact, the eta model retrieves a stronger FULL flow (95%) than the ECMWF because of the 34% CLIMO (Opal is analyzed slightly farther north) and 46% CYCLO contributions. Note that the eta ANTI contribution is smaller than the ECMWF by 4% (a large decrease is also evident in the 0000 UTC 5 October eta analysis - not shown), indicative of the systematic trend discussed below.

5.2.2 Eta Forecasts

a) Horizontal Geopotential and Wind Fields

The FULL geopotential field for the 12 and 48-h eta forecasts valid at 1200 UTC 5 October are presented in Figs. 5.6a and 5.7a, respectively. [The 24 and 36-h forecasts for this time, and all valid at 0000 UTC 5 October, reveal similar trends and are not presented]. The synoptic features in Fig. 5.6a are positioned similarly to the eta analysis (Fig. 5.4a) though the deep-layer geopotential of the western low is underforecast by 5 dam because of the CYCLO field (Fig. 5.6b). The eastern upper low also forms a closed circulation in the forecast that is absent in the analysis. The appearance of the closed cell weakens the CYCLO contribution along the mid-Atlantic coast with a corresponding

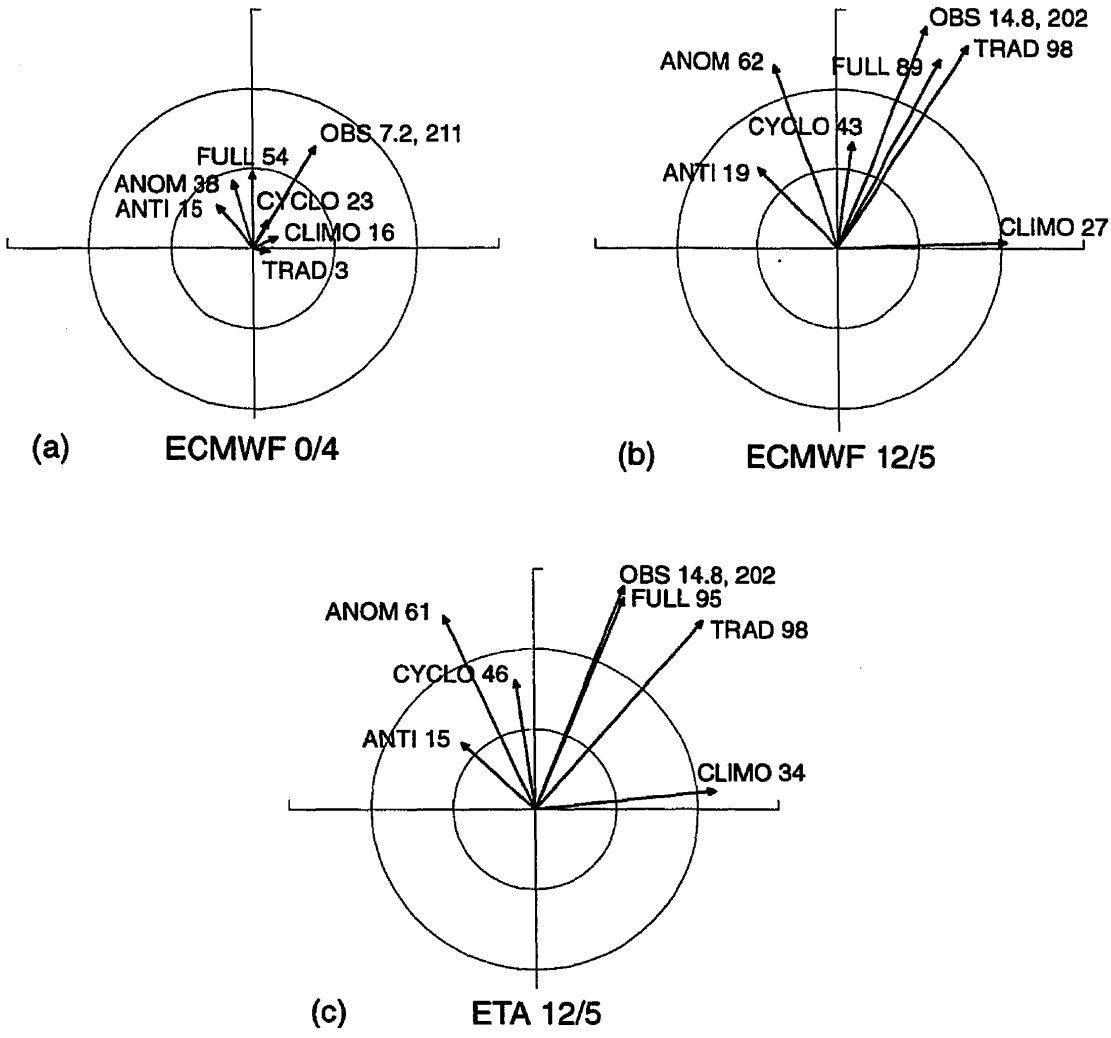

Fig. 5.5. Vector plots of the components of the steering flow for given times (hour/day), with panels (a), (b) and (c) corresponding to Figs. 5.2 to 5.4, respectively. Averaging is from 850-300 hPa over the domain of Opal's PSA. Numbers are percentages of the observed motion vector (OBS in m s^{-1} and degrees). TRAD is the deep-layer 5-7° annular average. Inner (outer) concentric circle represents 5 m s^{-1} (10 m s^{-1}) winds.

Table 5.1

Time/Date	Model	CLIMO (%)	CYCLO (%)	ANTI (%)	ANOM (%)	FULL (%)	TRAD (%)	RATIO
0000/4/F00	ECMWF	16	23	15	38	54	3	1.6
1200/5/F00	ECMWF	27	43	19	62	89	98	2.3
"	eta	34	46	15	61	95	98	3.2
0000/5/F12	"	32	51	12	63	95	74	4.3
1200/3/F48	"	21	47	-11	36	57	52	-4.2

Components of the steering flow as percentages of the observed storm motion (OBS) for different times and model runs. The vector OBS is 7.2 m s^{-1} from 211° at 0000 UTC 4 October and 14.8 m s^{-1} from 202° at 1200 UTC 5 October.

Fig. 5.6. As in Fig. 5.2, except for 12-h eta forecast valid at 1200 UTC 5 October. Opal is denoted by the 'L' in Alabama.

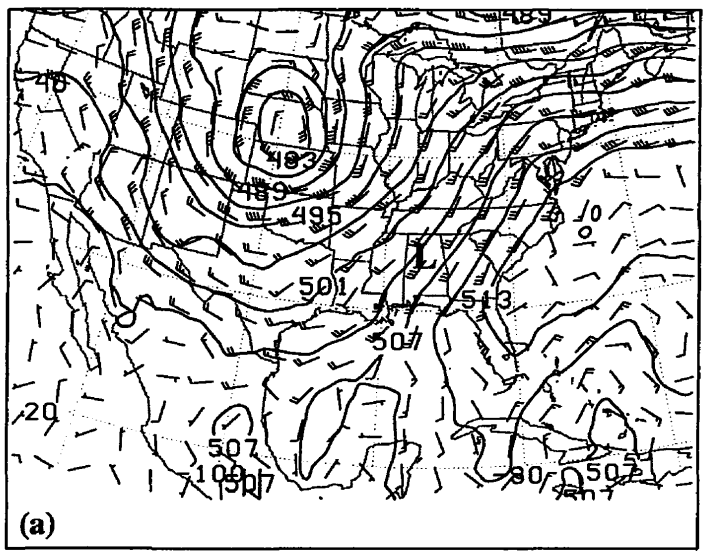

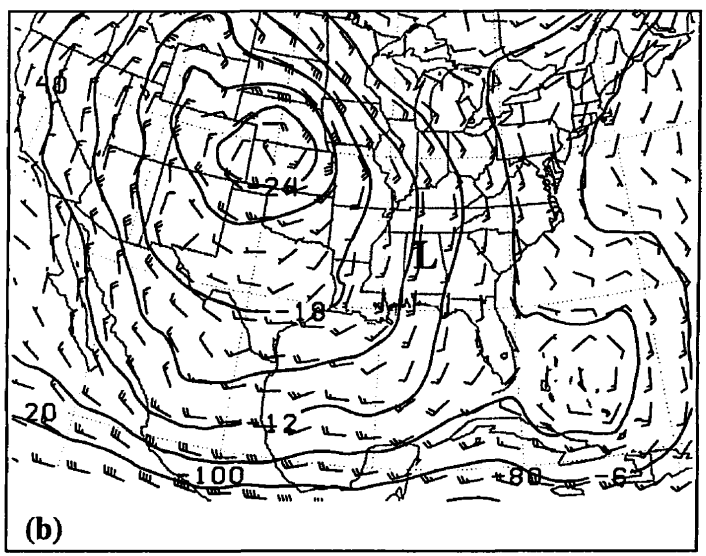

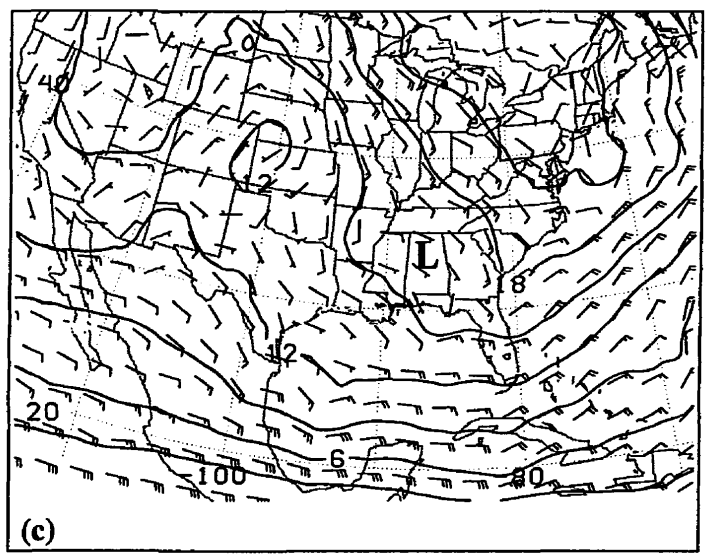

increase in the FULL eastern ridge (Fig. 5.6a) to 516 dam off Cape Hatteras. [While not influential in this study's inversion procedure, the TRAD vector may suffer from such a height pattern inconsistency]. Of further interest is the closed ANTI circulation located over Ohio in Fig. 5.4c that is absent in the forecast in Fig. 5.6c. This results in a weaker gradient and ANTI contribution over Opal (see section 5.2.2b).

The FULL 48-h forecast (Fig. 5.7a) places a western low of similar intensity to that of the analysis but located too far east in eastern Nebraska. As well, the eastern ridge lies farther offshore the southeast coast though differences are otherwise unremarkable. The eastern upper low is again weaker in Fig. 5.7b than in Fig. 6b, and while the 48-h forecast of the western low is similar to the analysis (unlike the 12-h forecast), the effect on Opal's steering flow is small. The ANTI contribution (Fig. 7c), however, continues to decrease with now only a weak *zonal* flow over Opal. Anomalous geopotentials are lower over the entire eastern U.S. with the closest closed anticyclonic circulation now distant over New England. The ridge over Florida is less defined and there is an easterly flow over Opal induced by the ridge extension from Arkansas to Indiana.

b) Vector Wind Fields

The 12-h forecast vector plot valid at 1200 UTC 5 October in Fig. 5.8a shows that ANTI continues to decrease and is now 12% of OBS. CYCLO has veered slightly and increased to 51%, higher than in the analysis. These, along with a decrease in CLIMO owing to a forecasted position farther south, account for the unchanged 95% retrieval.

The 48-h forecast vector plot (Fig. 5.8b) shows a much reduced CLIMO steering component of 21%, again because of a more equatorward position over the Florida panhandle. ANTI is now *large and negative (-11%)*, indicating that this contribution is now hindering Opal's northeastward motion (i.e., without the eastern ridge, Opal would be advancing faster poleward). The poor representation of the eastern ridge is responsible

Fig. 5.7. As in Fig. 5.2, except for 48-h eta forecast valid at 1200 UTC 5 October. Opal is denoted by the 'L' over the Florida panhandle.

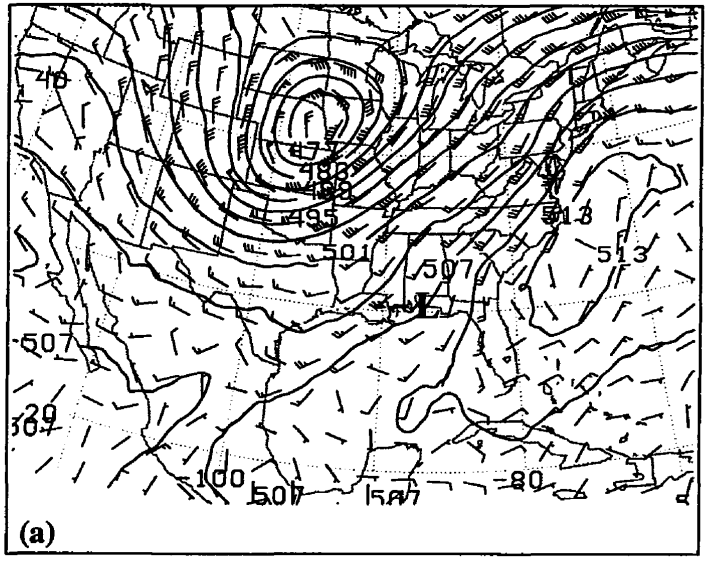

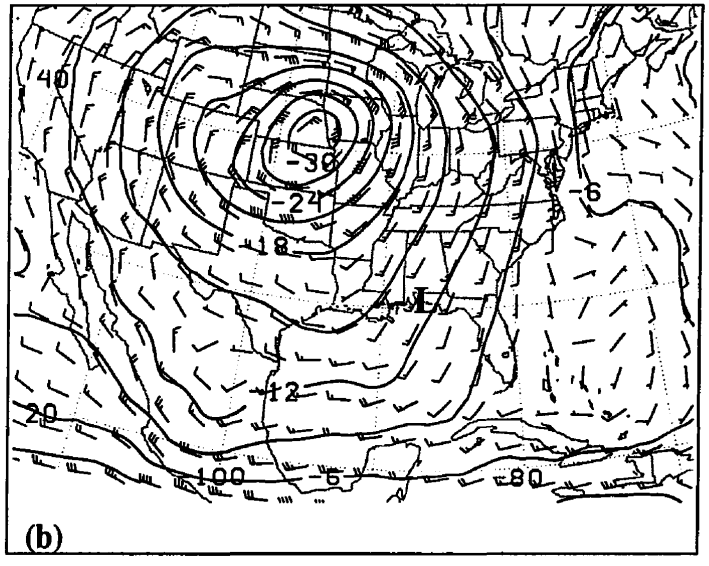

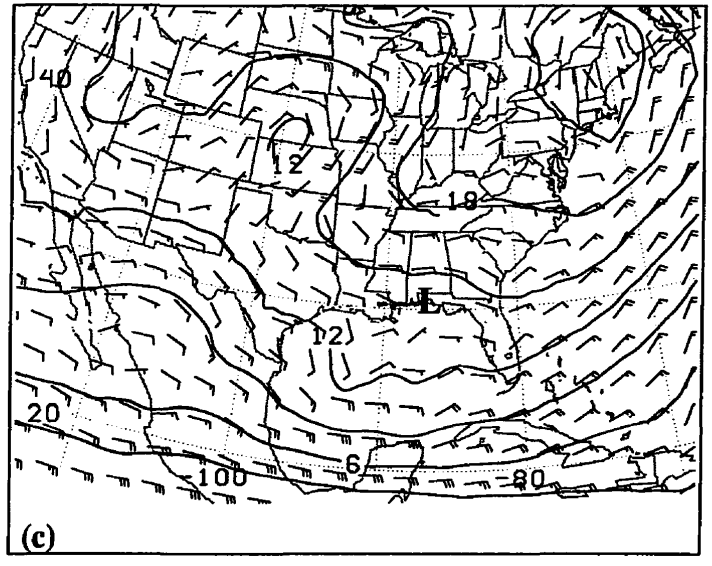

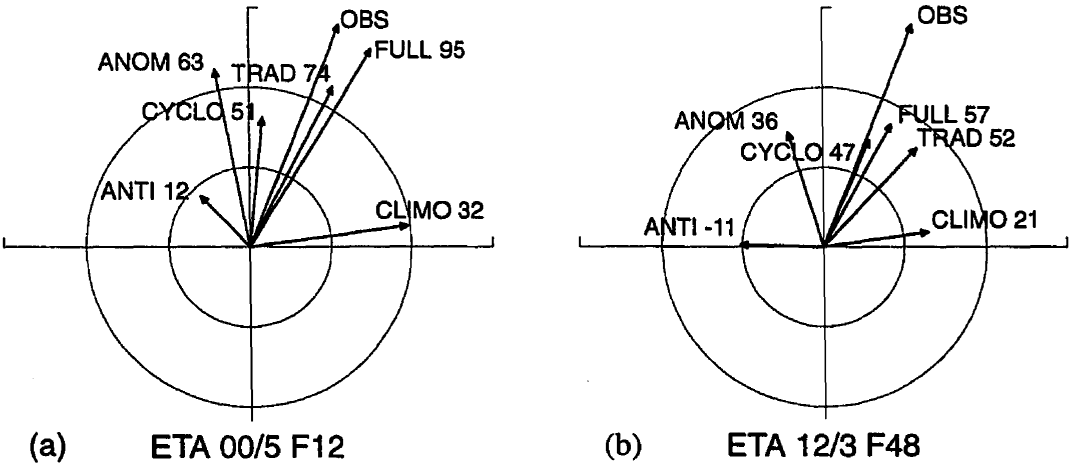

Fig. 5.8. As in Fig. 5.5, except for eta model forecasts of (a) 12-h (F12) and (b) 48-h (F48), valid at 1200 UTC 5 October, corresponding to Figs. 5.6 and 5.7. The observed motion vector OBS is 14.8 m s^{-1} from 202°.

for the trend of the decreasing, and becoming negative, ANTI contribution. [Interpretation is given in the following three sections]. The trend is the only one indicative of poor model representation of a physical feature. FULL, as a result, retrieves only 57% of OBS. Because of the poor representation of the ridge, the 48-h forecast is approximately 12 h, or about 600 km, too slow with the position of Opal. The 'missed flow' components of ANTI between Figs. 5.8b and 5.5b (the ECMWF analysis), and Figs. 5.8b and 5.5c (the eta analysis), of 4.4 m s^{-1} and 3.8 m s^{-1}, respectively, acting over 48 h, would advect Opal farther along its northeastward path by 767 km and 665 km, respectively. The missing ANTI component alone can explain the slow track forecast.

5.2.3 Thickness Field Forecast Errors

To evaluate the vertical structure of the eta forecasts, particularly of the eastern ridge, we present 48-h forecast errors (forecast minus analyzed) of anomalous thickness (observed minus climatology) valid at 1200 UTC 5 October. Regions of positive (negative) anomaly were forecasted too warm (cold). The 48-h forecasts are representative and exhibit a robust thermal anomaly signature.

The deep-layer (850-300 hPa) observed thickness at 1200 UTC 5 October (Fig. 5.9a) shows an extensive warm anomaly over the eastern U.S. and southeastern Canada that was underforecast by as much as 7 dam (Fig. 5.9b) along the southeast U.S. coast and mid-Atlantic states. The strong error in southwestern Minnesota (Fig. 5.9b) appears in Fig. 5.9c as a strong geopotential dipole in the central Plains caused by the phase speed error of the western low. The +8 dam Gulf coast error in Fig. 5.9b was caused by advection by Opal's cyclonic gyre of the baroclinic environment (Fig. 5.9c); cold advection had replaced the tropical air mass forecasted to be over the Gulf coast states. As well, overforecasted thicknesses are seen east of the Bahamas in Fig. 5.9c. Figure 5.9d shows that the error in the downstream ridge of more than 7 dam is largely due

Fig. 5.9. Deep-layer (850-300 hPa) observed thickness anomalies and forecast errors (forecast minus observed). Panel (a) is the observed eta thickness anomaly field at 1200 UTC 5 October. Panels (b), (c) and (d) are the ANOM forecast error (sum of (c) and (d)), CYCLO and ANTI, respectively. In (a) the contour interval is 3 dam, and 1 dam in (b) and (c), plotted when the magnitude of the error is greater than 4 dam. The northern 'L' is the 1200 UTC 5 October eta analyzed position of Opal; the southern 'L' is the 48-h forecasted position.

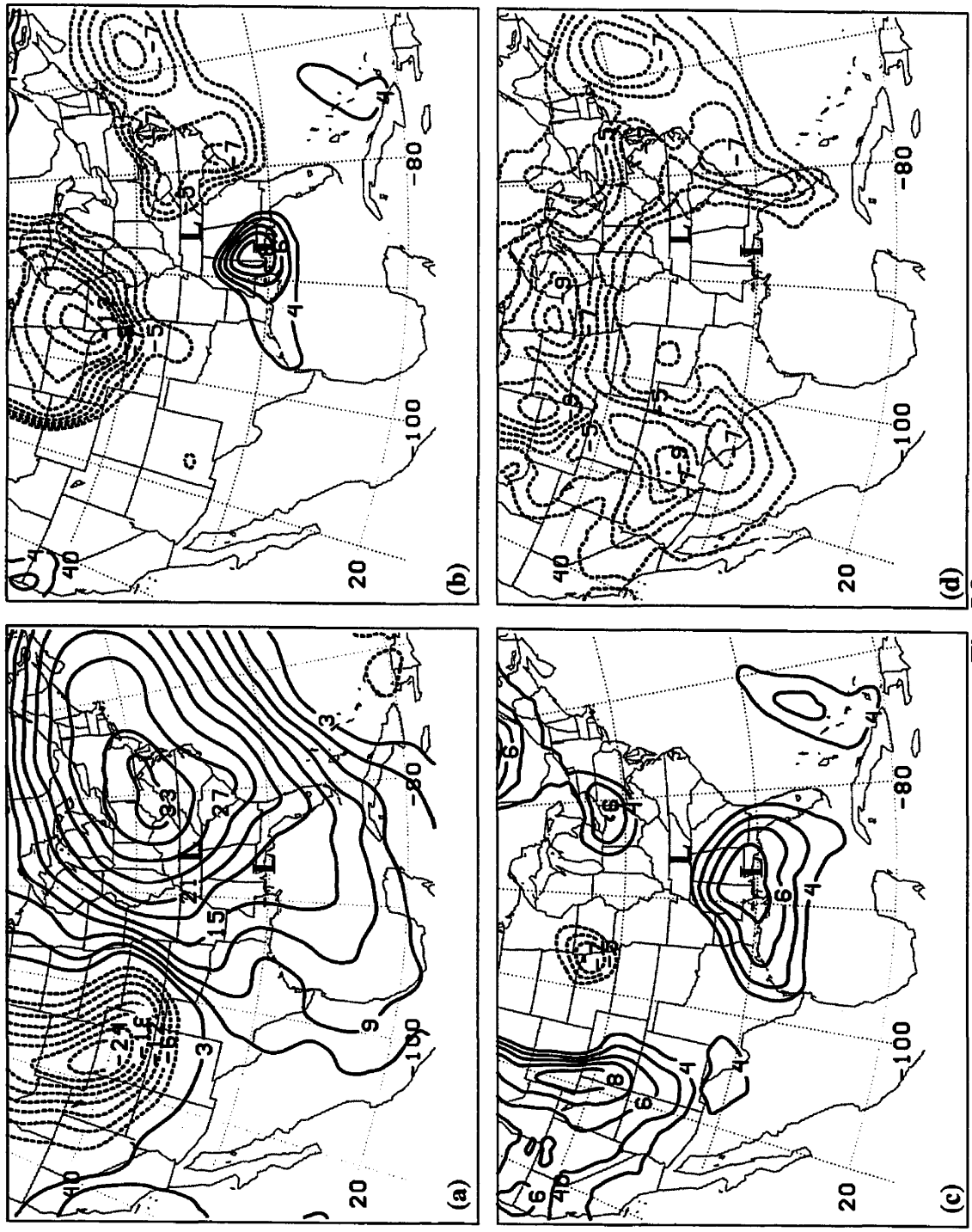

Fig. 5.9

to the effects of ANTI (i.e., Opal's phase speed was unimportant in the underforecast eastern ridge; see the lack of strong error along the U.S. east coast in Fig. 5.9c).

We now divide the errors into upper levels (500-300 hPa, Fig. 5.10) and lower levels (850-500 hPa, Fig. 5.11). The anomalous upper thickness field at 1200 UTC 5 October (Fig. 5.10a) shows an elongated maximum above 15 dam in West Virginia just northeast of the analyzed position of Opal. Comparing Figs. 5.10b (CYCLO plus ANTI), 5.10c (CYCLO) and 5.10d (ANTI) with the corresponding lower-level anomalies in Figs. 5.11b, 5.11c and 5.11d, confirms that low-level cyclonic advection contributes significantly to the positive error southwest of Opal. ANTI errors at low-levels (Fig. 5.11d) are more distinct along the U.S. east coast, likely associated with the passage of the low-level warm front created by warm advection east of Opal (Fig. 2.4d).

Areas of significant upper-level underforecasted thicknesses are found in flow that was once in the vicinity of Opal. The 4 dam error in western Ohio (magnitude not fully resolved in Fig. 5.10d) is colocated with the local maximum in ANTI-induced geopotential in Fig. 5.4c, suggesting that *upper level anticyclonic processes* were responsible for the increased southeasterly flow over Tennessee and Virginia. The extension of the ridge over Florida and the coastal southeast states contributes less.

5.2.4 Discussion

The ability of the QGPV inversion procedure to retrieve the overall synoptic pattern of a western low and eastern ridge has been shown for both datasets. Because the ECMWF's overall performance was better, we consider those analyses (Figs. 5.2 and 5.3) to be the synoptic-scale 'ground truth' representations of the atmosphere. This may be expected since the ECMWF's data cutoff time of +3 h (Escoffier and Provost 1995) is longer than the early eta's +1.25 h (Rogers et al. 1995), thus including more data. On the other hand, the merit of the early eta needs to be evaluated since it provides the earliest possible operational numerical guidance. The eta analysis of 1200 UTC 5 October

Fig. 5.10. As in Fig. 5.9, but for upper anomalies (500-300 hPa).

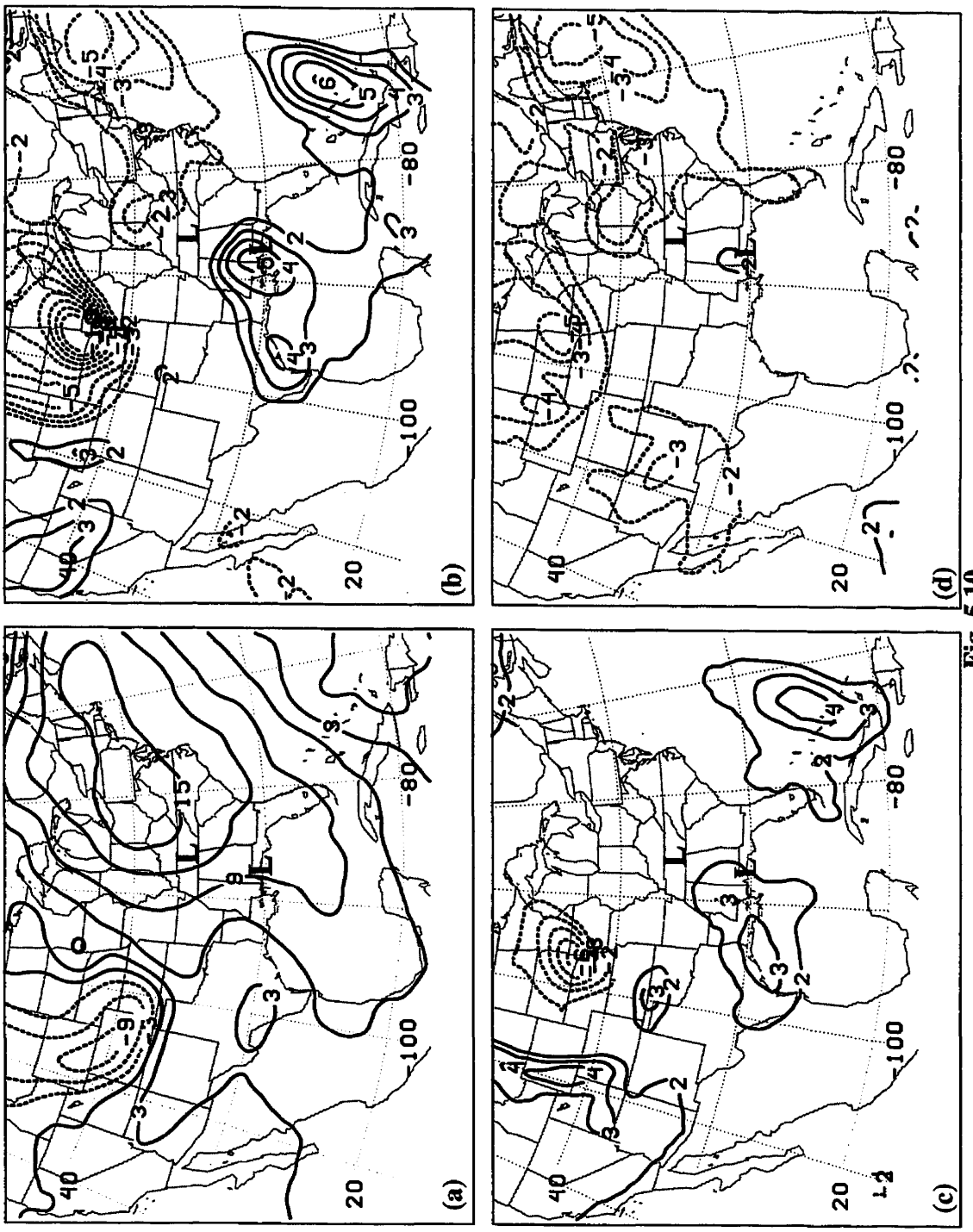

Fig. 5.10

Fig. 5.11. As in Fig. 5.9, but for lower anomalies (850-500 hPa).

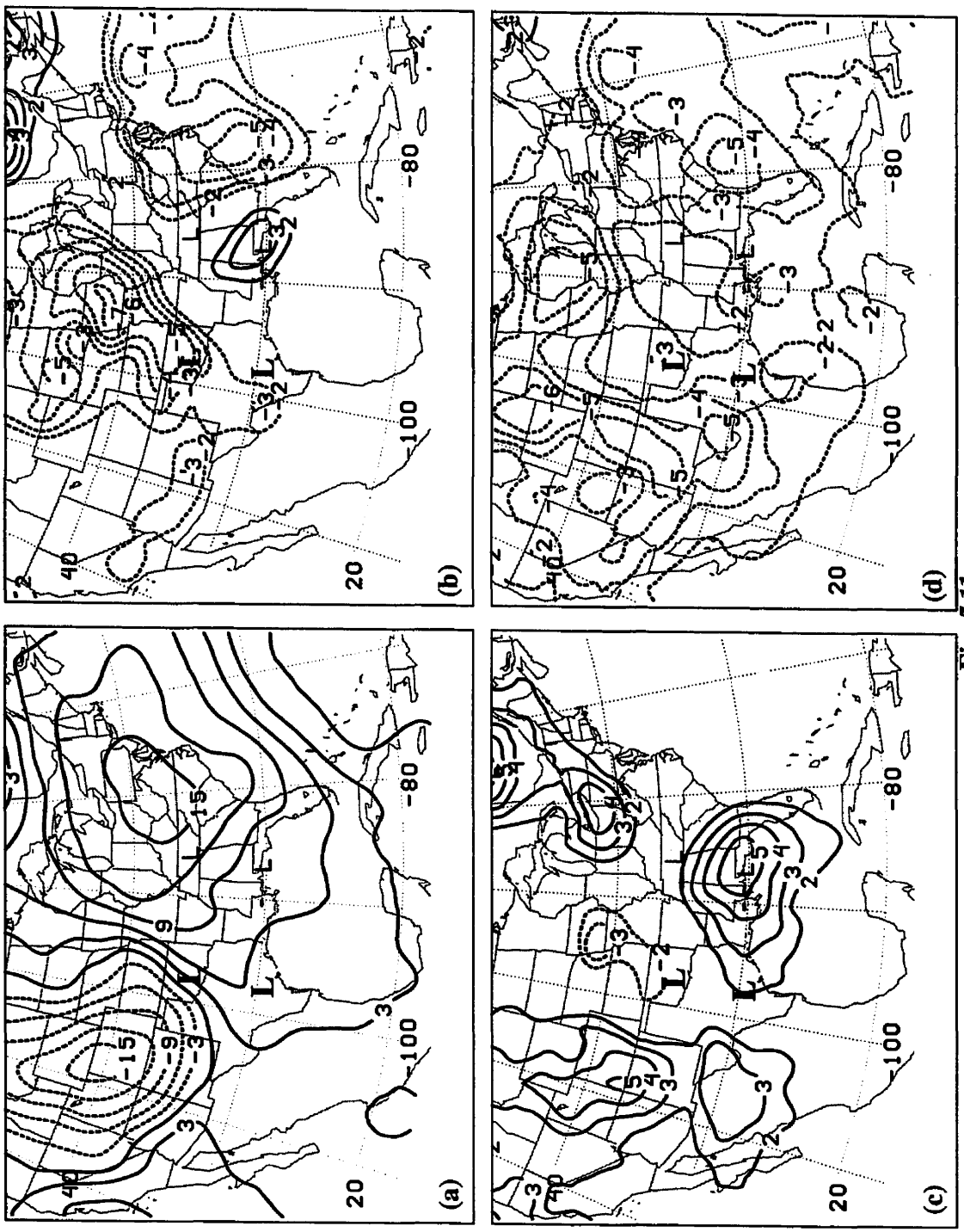

Fig. 5.11

compares well with the ECMWF but hints at a reduced ANTI contribution and thus poor representation of the ridge. This inadequacy (also seen in earlier eta analyses, not shown) propagates through the forecasts.

The FULL vector was generally superior to TRAD because the TRAD method relies upon the (improbable) realistic representation of the hurricane's height field by a synoptic-scale model and analysis system. The inversion technique in this study uses the much better-resolved environment following removal of the storm's circulation. As well, the QGPV inversion method may be even more valuable during weaker or more chaotic steering regimes as at 0000 UTC 4 October (TRAD accounted for 3 % versus 54 % by FULL). This is likely due to averaging of the height field from more than one synoptic feature which makes the choice of radii involved critical. This situation is more likely when the storm is in the sub-tropics or when recurvature is imminent or has just occurred. As well, TRAD did not exhibit a systematic bias with respect to FULL.

The better shorter-term forecasts of storm motion (e.g., the 12-h versus 48-h shown) may be a result, in part, of the positioning of Opal farther north within a region of larger geopotential gradient between the western low and eastern ridge. This may explain the stronger 24-h (not shown), 12-h and analysis CYCLO contributions valid at 1200 UTC 5 October. However, a 'missing flow' from a misrepresented physical feature, here found to be ANTI, needed to have advected the storm farther north in the first place. The ANTI-induced flow became strongly meridional from the 48 to 12-h forecasts, thus 'catching' the storm up to its analyzed position.

The increase in CLIMO flow farther north in the westerlies is a secondary cause since CLIMO is stronger over Tennessee than over the panhandle of Florida by 13%. Note that this flow, however, is almost zonal so CLIMO can only contribute a signficant eastward component.

It was observed that later eta model runs (both forecasts and analyses) steadily improved their representation of the anticyclonic contribution with respect to the ECMWF, especially for runs issued as the storm made landfall near 0000 UTC 5 October. This was the only significant trend seen in the steering flow components.

The dense U.S. upper air observing network, compared with that in the Gulf of

Mexico, very likely improved the steering flow retrievals beginning at 0000 UTC 5 October and readily apparent as the storm was becoming extratropical 12 h later. Indeed, the retrieved flow from the 0000 UTC 4 October ECMWF analysis was the poorest of all inversions. Increasingly during the entire period of study, the storm's outflow and associated high tropopause (Figs. 2.2b through 2.4b) was advected over the relatively dense upper air sites of the southeast U.S. Satellite images at this time showed a broad cirrus deck streaming to the east and northeast of Opal (Fig. 5.12). With better representation of the outflow in the analyses possible at 0000 UTC 5 October, the 12-h forecast (valid at 1200 UTC 5 October) predicted a significantly more pronounced ridge extending into Florida. Shapiro (1996) and Wu and Kurihara (1996) have emphasized the need for enhanced upper air observations and accurate analysis for better prediction of storm movement. In strong support of this hypothesis, Burpee et al. (1996) showed that the release of Omega dropwindsondes in the vicinity of tropical systems significantly reduces the mean forecast errors of operational hurricane track forecast models.

5.2.5 Evidence of the Contribution to the Eastern Ridge Building by Opal's Outflow

While the downstream ridge has been identified as being the key factor in the poor forecast (i.e., ANTI was large and negative in the 48-h forecast), we now present evidence that Opal's poorly analyzed and modelled outflow contributed to the ridge building.

The ECMWF at 0000 UTC on 4 and 5 October (not shown) and 1200 UTC 5 October resolved a local maximum of ANTI anomalous positive geopotential at, or within, 10° latitude downstream of Opal that increased in intensity through the period. The eta model's closest maxima, however, was distant until 1200 UTC 5 October, 12 h following landfall over a dense network of upper air sites. The close proximity of the downstream ridge increased the height gradient and thus southerly flow over the storm. Earlier studies, through deliberate exclusion (instead of paucity of upper air data) of a

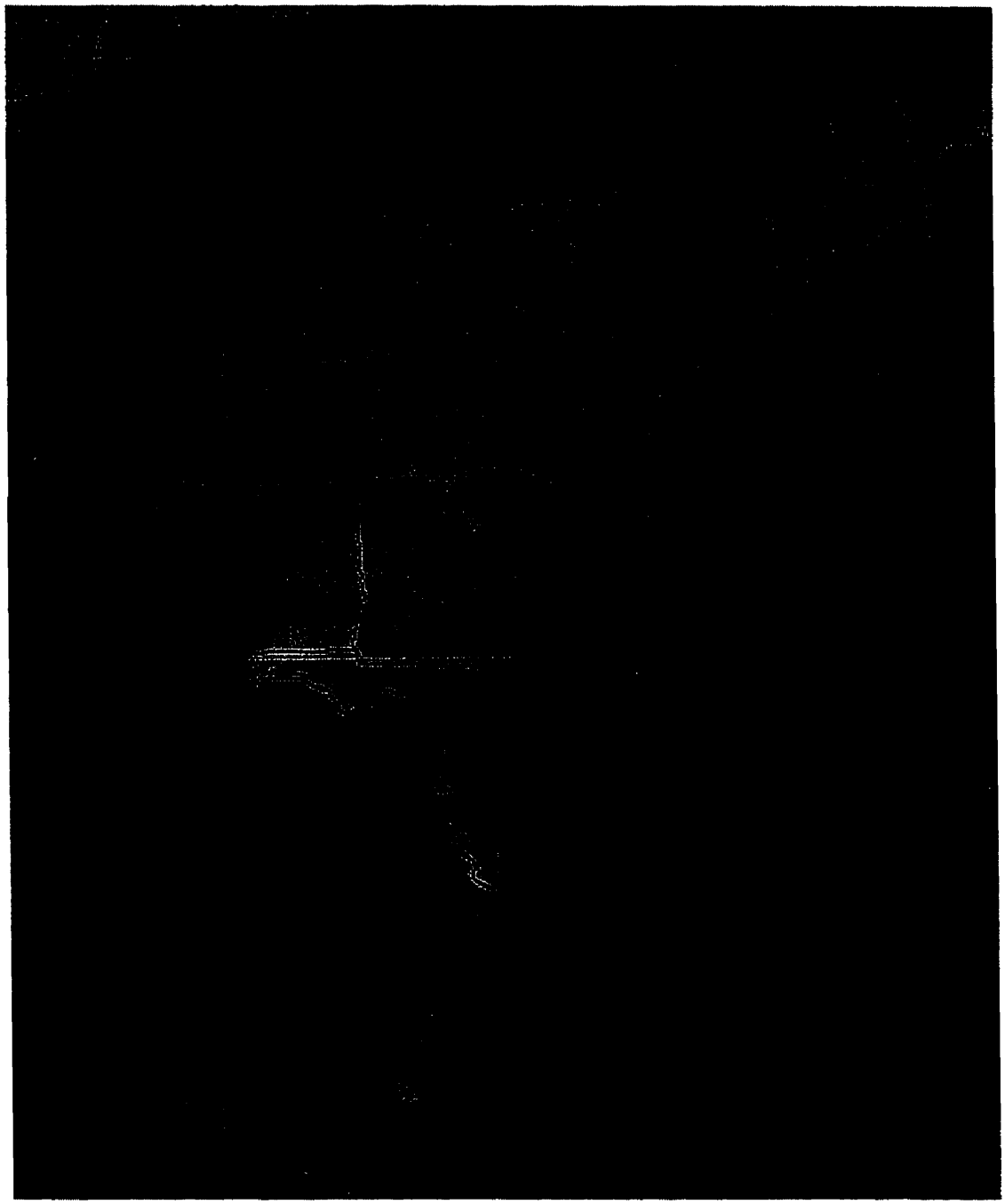

Fig. 5.12. Infrared satellite image at 2345 UTC 4 October. Opal is over the Florida panhandle.

hurricane and outflow, have shown modification of the environment by the outflow. Ross and Kurihara (1995) observed the ridge downstream of Hurricane Gloria to be more intense and positioned closer to the storm when Gloria was included in their numerical simulation than when it was absent.

A right bias of FULL with respect to OBS (average of 5° for the ECMWF (5 October only) and 13° for the eta) is seen for all except one analysis and forecast. The exception was the 31° leftward deviation in the ECMWF 0000 UTC 4 October analysis. These biases (FULL versus OBS) are comparable in magitude but opposite in direction to earlier studies comparing TRAD versus OBS (George and Gray 1976; Dong and Neumann 1986). This study's FULL-OBS bias may be explained by the eta's under-representation of hurricane-to-environment interaction. Pielke (1990) states that outflow in the right front (with respect to its forward motion) quadrant of a hurricane will build the downstream ridge with the storm moving to the left of the track uninfluenced by outflow effects. The well-defined cirrus canopy (Merritt and Wexler 1967; Pielke 1990) rapidly advected northeastward well ahead of Opal (Fig. 5.12). Similarly, Pielke states that mass accumulation due to outflow located in the right rear quadrant (where the anticyclonic gyre of tropopause winds indicates low-potential vorticity upper level outflow in Fig. 2.4) will accelerate the storm to the north. Wu and Kurihara (1996) showed that the negative upper-level EPV anomaly downstream of Hurricane Bob induced a southeasterly flow of about 3 m s^{-1} over the storm which is similar in magnitude to this study's missing ANTI flow. This supports the notion that the eta model severely under-represented Opals' upper level outflow and its effect on building the downstream ridge.

We have presented evidence that poor analysis (before the storm's outflow passed over the U.S.) and subsequent modelling of the eastern ridge lead to a significantly slow forecast. The above discussion raises the related issue of how *unexpected storm intensification* can similarly lead to a poor track forecast (K. Emanuel 1997, personal communication) after a time lag of perhaps 1/2 to 2 d. This is sufficient time for the unexpectedly strong upper-level EPV anomaly to be advected downstream by the environmental vertical shear and to induce a steering flow. Future research must therefore treat storm intensity and short-term storm track as being intimately related.

Chapter 6

Summary and Future Applications

Hurricane Opal was a major hurricane that made landfall near Pensacola, Florida at 2200 UTC 4 October 1995. The underprediction by NCEP's eta model of the storm's forward speed through the time of landfall and passage into the interior eastern U.S. motivated this study. The rapid (and unexpected) deepening of Opal 12 h prior to landfall and underforecast forward motion emphasized the need for accurate forecasts of hurricane motion.

Goal 1: We identify a quasi-stationary ridge over the eastern U.S. and an eastward-advancing extratropical cyclone as defining the environmental flow around Opal from 0000 UTC 4 October to 1200 UTC 5 October. A southerly flow between these features from the Gulf of Mexico to the Great Lakes steered Opal north-northeastwards.

Goal 2: The QGPV inversion procedure retrieved a significant percentage of the observed flow. Between 89% and 103% of the observed storm motion during, and after, landfall was accounted for. However, retrieval of the steering flow is highly dependent upon the quality of the environmental analysis; the analysis from 0000 UTC 4 October accounted for only 54% of the observed motion owing to the paucity of upper air data in the Gulf of Mexico.

Goal 3: The ECMWF analyses generally retrieved a larger component (average of 96% of OBS for 5 October) of the steering flow than did the eta model (81%) and so were considered to be the 'ground truth' representations of the atmosphere. [The eta analyses provided a valuable ceiling to the performance of the eta forecasts]. The purpose of the 'early' eta to give the earliest available numerical guidance to operational forecasters likely explains the eta's inferior performance, regardless of numerical and physical model differences. Even so, it is encouraging that this study's straightforward systematic procedure can be successfully applied to unmodified model output that is traditionally consulted by operational forecasters.

Goal 4: The eastern ANTI-induced ridge was persistently forecasted too weak and too distant from the storm's position, resulting in a too weak ANTI component. Compared to the eta analysis' 15% ANTI contribution, in all but one of the forecasts this component was negative (e.g., -11% at 48 h), thus inhibiting the north-northeastward storm motion over 48 h by 26%. The exception was the 12-h forecast valid at 1200 UTC 5 October (12%) that typified the trend towards the analysis' value at shorter forecast ranges (12 and 24 h). The 'missing' eta flow (analysis minus 48-h forecast) of 3.8 m s^{-1} is sufficient over 48 h to advect the storm to its observed position.

The CLIMO component exhibited positive feedback by increasing as Opal was placed repeatedly farther north. This important trend accounted for 13% of the increase in FULL over 48 but was not associated with poor modelling. The contribution was mostly zonal and so was incapable itself of locating the storm farther north.

Goal 5: Hurricane-to-environment effects were likely a major contributor to the underforecasted ridge building over the eastern U.S. The divergent low potential vorticity outflow air was spread northeast then east by 15-40 m s^{-1} tropopause winds, in a manner similar to the theory of Wu and Emanuel (1993, 1994). The storm's condensational heating thus indirectly warmed (increased θ_T) the upper troposphere (as seen by Davis et al 1993; Morgan 1996; Stoelinga 1996) over Opal and downstream over the northeast U.S. and east coast at distances far greater than the storm's near-surface effects. Because

the storm's outflow was the source of the ridge building, the ridge became phase locked, more intense and intimately positioned over Ohio and the mid-Atlantic states (in the eta) and just off the coast (in the ECMWF). The magnitude of the intensification was missed by the eta model by up to 4 dam in the upper level thicknesses in the same region. Only when the outflow became well established over land did the more abundant upper air data result in more realistic analyses and similarly improved forecasts.

The results of this study encourage the operational use of QGPV inversion to identify real time synoptic steering features. We restate the need for more detailed upper air soundings and analyses to resolve the upper level physical processes associated with hurricanes. Furthermore, we emphasize the relationship between storm intensity and subsequent storm track. With future improvements in data collection and further development of numerical models, such as the 48-km early eta model (implemented on 12 October 1995 (Rogers et al. 1996)) and the introduction of the 29-km resolution meso-eta model (Black 1994), more timely warnings will diminish the continuing threat of hurricanes.

References

AMS, 1986a: Statement of Concern: Is the United States headed for hurricane disaster? *Bull. Amer. Meteor. Soc.*, **67**, 537-538.

_____, 1986b: Policy Statement: Hurricane detection, tracking, and forecasting. *Bull. Amer. Meteor. Soc.*, **67**, 1508-1510.

_____, 1993: Policy Statement: Hurricane detection, tracking, and forecasting. *Bull. Amer. Meteor. Soc.*, **74**, 1377-1380.

Black, R. X., and R. M. Dole, 1993: The dynamics of large-scale cyclogenesis over the North Pacific Ocean. *J. Atmos. Sci.*, **50**, 421-442.

Black, T. L., 1994: The new NMC mesoscale eta model: Description and forecast examples. *Wea. Forecasting*, **9**, 265-278.

_____, D. G. Deaven, and G. J. DiMego, 1993: The step-mountain eta-coordinate model: 80 km "early" version and objective verifications. NWS Technical Procedures Bull. 412, National Oceanic and Atmospheric Administration/National Weather Service, 31 pp. [Available from National Weather Service, Office of Meteorology, 1325 East-West Highway, Silver Spring, MD 20910.]

Bosart, L. F., and J. A. Bartlo, 1991: Tropical storm formation in a baroclinic environment. *Mon. Wea. Rev.*, **119**, 1979-2013.

_____, and G. M. Lackmann, 1995: Postlandfall tropical cyclone reintensification in a weakly baroclinic environment: A case study of Hurricane David (September 1979). *Mon. Wea. Rev.*, **123**, 3268-3291.

Bowie, E. H., 1922: Formation and movement of West Indian hurricanes. *Mon. Wea. Rev.*, **50**, 173-179.

Bresky, W. C., and S. J. Colucci, 1996: A forecast and analyzed cyclogenesis event diagnosed with potential vorticity. *Mon. Wea. Rev.*, **124**, 2227-2244.

Brinkmann, W. A. R., 1975: Hurricane hazard in the United States: a research assessment. Program on Technology, Environment and Man Monograph NSF-RA-E-75-007, Institute of Behavioral Science, The University of Colorado, 100 pp. [Available from the National Technical Information Service, U.S. Dept. of Commerce, Springfield, VA 22161.]

Burpee, R. W., J. L. Franklin, S. J. Lord, R. E. Tuleya, and S. D. Aberson, 1996: The impact of Omega dropwindsondes on operational hurricane track forecast models. *Bull. Amer. Meteor. Soc.*, **77**, 925-933.

Chan, J. C.-L., 1985: Identification of the steering flow for tropical cyclone motion from objectively analyzed wind fields. *Mon. Wea. Rev.*, **113**, 106-116.

_____, and W. M. Gray, 1982: Tropical cyclone movement and surrounding flow relationships. *Mon. Wea. Rev.*, **110**, 1354-1374.

_____, and R. T. Williams, 1987: Analytic and numerical studies of the beta-effect in tropical cyclone motion. Part 1: Zero mean flow. *J. Atmos. Sci.*, **44**, 1257-1264.

Charney, J. G., 1955: The use of primitive equations of motion in numerical prediction. *Tellus*, **7**, 22-26.

_____, and M. E. Stern, 1962: On the stability of internal baroclinic jets in a rotating atmosphere. *J. Atmos. Sci.*, **19**, 159-172.

Davis, C. A., 1992a: Piecewise potential vorticity inversion. *J. Atmos. Sci.*, **49**, 1397-1411.

_____, 1992b: A potential-vorticity diagnosis of the importance of initial structure and condensational heating in observed extratropical cyclogenesis. *Mon. Wea. Rev.*, **120**, 2409-2428.

_____, and K. A. Emanuel, 1991: Potential vorticity diagnostics of cyclogenesis. *Mon. Wea. Rev.*, **119**, 1929-1953.

_____, M. T. Stoelinga, and Y-H Kuo, 1993: The integrated effect of condensation in numerical simulations of extratropical cyclogenesis. *Mon. Wea. Rev.*, **121**, 2309-2330.

DeMaria, D., M. B. Lawrence, and J. T. Kroll, 1990: An error analysis of Atlantic tropical cyclone track guidance models. *Wea. Forecasting*, **5**, 47-61.

Dong, K., and C. J. Neumann, 1986: The relationship between tropical cyclone motion and environmental geostrophic flows. *Mon. Wea. Rev.*, **114**, 115-122.

Elsberry, R. L., 1995: Tropical cyclone motion. WMO Tropical Meteorological Research Programme. *Proc. of the Second WMO International Workshop on Tropical Cyclones (IWTC-II).* Manila, 1989, 27-53. [Available from WMO, Case Postale No. 2300, CH-1211 Geneva 2, Switzerland.]

Ertel, H., 1942: Ein neuer hydrodynamischer wirbelsatz. *Meteor. Z.*, **59**, 277-281.

Escoffier, C., and C. Provost, 1995: Wind forcing over the southwest Atlantic: Comparison between observations and ECMWF analyses. *Mon. Wea. Rev.*, **123**, 1269-1287.

Fiorino, M., and R. L. Elsberry, 1989: Some aspects of vortex structure related to tropical cyclone motion. *J. Atmos. Sci.*, **46**, 975-990.

Franklin, J. L., S. E. Feuer, J. Kaplan, and S. D. Aberson, 1996: Tropical cyclone motion and surrounding flow relationships: searching for beta gyres in Omega dropwindsonde datasets. *Mon. Wea. Rev.*, **124**, 64-84.

George, J. E., and W. M. Gray, 1976: Tropical cyclone motion and surrounding parameter relationships. *J. Appl. Meteor.*, **5**, 1252-1264.

Hakim, G. J., L. F. Bosart, and D. Keyser, 1995: The Ohio-Valley wave-merger cyclogenesis event of 25-26 January 1978. Part I: Multiscale case study. *Mon. Wea. Rev.*, **123**, 2663-2692.

_____, D. Keyser, and L. F. Bosart, 1996: The Ohio-Valley wave-merger cyclogenesis event of 25-26 January 1978. Part II: Diagnosis using quasigeostrophic potential vorticity inversion. *Mon. Wea. Rev.*, **124**, 2176-2205.

Hoerling, M. P., T. K. Schaack, and A. J. Lenzen, 1991: Global objective tropopause analysis. *Mon. Wea. Rev.*, **119**, 1816-1831.

Holliday, C. R., and A. H. Thompson, 1979: Climatological characteristics of rapidly intensifying typhoons. *Mon. Wea. Rev.*, **107**, 1022-1034.

Holopainen, E., and J. Kaurola, 1991: Decomposing the atmospheric flow using potential vorticity framework. *J. Atmos. Sci.*, **48**, 2614-2625.

Hoskins, B. J., M. E. McIntyre, and A. W. Robertson, 1985: On the use and significance of isentropic potential vorticity maps. *Quart. J. Roy. Meteor. Soc.*, **111**, 877-946.

Huo, Z., D.-L. Zhang, and J. Gyakum, 1995: A diagnostic analysis of the superstorm of March 1993. *Mon. Wea. Rev.*, **123**, 1740-1761.

Jarrell, J. D., 1993: Hurricane fix-to-fix speed calculations. Preprints, *20th Conf. on Hurricanes and Tropical Meteorology*, San Antonio, TX, Amer. Meteor. Soc., 296-299.

Jordan, E. S., 1952: An observational study of the upper wind-circulation around tropical storms. *J. Meteor.*, **9**, 340-346.

Koch, S. E., M. desJardins, and P. J. Kocin, 1983: An interactive Barnes objective map analysis scheme for use with satellite and conventional data. *J. Climate Appl. Meteor.*, **22**, 1487-1503.

Lackmann, G. M., and J. R. Gyakum, 1996: Heavy cold-season precipitation in the northwestern United States: Climatology and a diagnosis of the flood of 17-18 January 1986. Preprints, *15th Conf. on Weather Analysis and Forecasting*, Norfolk, VA, Amer. Meteor. Soc., 265-268.

_____, _____, and R. Benoit, 1997: Moisture transport diagnosis of a wintertime precipitation event in the Mackenzie River Basin, *Mon. Wea. Rev.*, conditionally accepted.

Lamarque, J.-F., and P. G. Hess, 1994: Cross-tropopause mass exchange and potential vorticity budget in a simulated tropopause folding. *J. Atmos. Sci.*, **51**, 2246-2269.

Merrill, R. T., 1984: A comparison of large and small tropical cyclones. *Mon. Wea. Rev.*, **112**, 1408-1418.

_____, 1988: Characteristics of the upper-tropospheric environmental flow around hurricanes. *J. Atmos. Sci.*, **45**, 1665-1677.

_____, and C. S. Velden, 1996: A three-dimensional analysis of the outflow layer of Supertyphoon Flo (1990). *Mon. Wea. Rev.*, **124**, 47-63.

Merritt, E. S., and R. Wexler, 1967: Cirrus canopies in tropical storms. *Mon. Wea. Rev.*, **95**, 111-120.

Mesinger, F., Z. I. Janjic, S. Nickovic, D. Gavrilov, and D. G. Deaven, 1988: The step-mountain coordinate: Model description and performance for cases of Alpine lee cyclogenesis and for a case of an Appalachian redevelopment. *Mon. Wea. Rev.*, **116**, 1493-1518.

Miller, B. I., 1964: A study of the filling of Hurricane Donna (1960) over land. *Mon. Wea. Rev.*, **92**, 389-406.

_____, and P. L. Moore, 1960: A comparison of hurricane steering levels. *Bull. Amer. Meteor. Soc.*, **41**, 59-63.

Molinari, J., S. Skubis, and D. Vollaro, 1995: External influences on hurricane intensity. Part III: Potential vorticity structure. *J. Atmos. Sci.*, **52**, 3593-3606.

Morgan, M. C., 1996: On the dynamics of diabatically generated "outflow" during cyclogenesis. Preprints, *7th Conf. on Mesoscale Processes,* Reading, England, Amer. Meteor. Soc., 29-31.

Neumann, C. J., and J. M. Pelissier, 1981: Models for the prediction of tropical cyclone motion over the North Atlantic: An operational evaluation. *Mon. Wea. Rev.*, **109**, 522-538.

NHC, 1995: Hurricane Opal Preliminary Report, 14 pp. [Available from National Hurricane Center, 11691 SW 17th St., Miami, FL 33165-2149.]

Pauley, P. M., N. L. Baker, and E. H. Barker, 1996: An observational study of the Interstate 5 dust storm case. *Bull. Amer. Meteor. Soc.*, **77**, 693-720.

Pielke, R. A., 1990: The Hurricane. Routledge, New York. 228 pp.

Raymond, D. J., 1992: Non-linear balance and potential-vorticity thinking at large Rossby number. *Quart. J. Roy. Meteor. Soc.*, **118**, 987-1015.

Riehl, H., and N. M. Burgner, 1950: Further studies of the movement and formation of huricanes and their forecasting. *Bull. Amer. Meteor. Soc.*, **31**, 244-253.

Robinson, W. A., 1988: Analysis of LIMS data by potential vorticity inversion. *J. Atmos. Sci.*, **45**, 2319-2342.

Rogers, E., D. G. Deaven, and G. J. DiMego, 1995: The regional analysis system for the operational eta model: Original 80-km configuration and recent changes. *Wea. Forecasting*, **10**, 810-825.

_____, T. L. Black, D. G. Deaven, G. J. DiMego, Q. Zhao, M. Baldwin, N. W. Junker and Y. Lin, 1996: Changes to the operational "early" eta analysis/forecast system at the National Centers for Environmental Prediction. *Wea. Forecasting*, **11**, 391-413.

Ross, R. J., and Y. Kurihara, 1995: A numerical study on influences of Hurricane Gloria (1985) on the environment. *Mon. Wea. Rev.*, **123**, 332-346.

Sadler, J. C., 1976: A role of the tropical upper tropospheric trough in early season typhoon development. *Mon. Wea. Rev.*, **104**, 1266-1278.

Shapiro, L. J., 1996: The motion of Hurricane Gloria: A potential vorticity diagnosis. *Mon. Wea. Rev.*, **124**, 2497-2508.

_____, and J. L. Franklin, 1995: Potential vorticity in Hurricane Gloria. *Mon. Wea. Rev.*, **123**, 1465-1475.

Sheets, R. C., 1990: The National Hurricane Center - Past, present, and future. *Wea. Forecasting*, **5**, 185-232.

Simpson, R. H., 1974: The hurricane disaster potential scale. *Weatherwise*, **27**, 169-186.

Stoelinga, M. T., 1996: A potential vorticity-based study of the role of diabatic heating and friction in a numerically simulated baroclinic cyclone. *Mon. Wea. Rev.*, **124**, 849-874.

Trenberth, K. E., 1992: Global analyses from ECMWF and atlas of 1000 to 10-mb circulation statistics. NCAR Tech. Note NCAR/TN-373 + STR, 191 pp., plus 24 fiche.

Velden, C. S., 1993: The relationship between tropical cyclone motion, intensity and the vertical extent of the environmental steering layer in the Atlantic basin. Preprints, *20th Conf. on Hurricanes and Tropical Meteorology*, San Antonio, TX, Amer. Meteor. Soc., 31-34.

_____, and L. M. Leslie, 1991: The basic relationship between tropical cyclone intensity and the depth of the environmental steering layer in the Australian region. *Wea. Forecasting*, **6**, 244-253.

Wakimoto, R. M., and P. G. Black, 1994: Damage survey of Hurricane Andrew and its relationship to the eyewall. *Bull. Amer. Meteor. Soc.*, **75**, 189-200.

Whitfield, M. B., and S. W. Lyons, 1992: An upper-tropospheric low over Texas during summer. *Wea. Forecasting*, **7**, 89-106.

Willoughby, H. E., and P. G. Black, 1996: Hurricane Andrew in Florida: dynamics of a disaster. *Bull. Amer. Meteor. Soc.*, **77**, 543-549.

_____, J. A. Clos, and M. G. Shoreibah, 1982: Concentric eye walls, secondary wind maxima, and the evolution of the hurricane vortex. *J. Atmos. Sci.*, **39**, 395-411.

Wu., C. C., and K. A. Emanuel, 1993: Interaction of a baroclinic vortex with background shear: Application to hurricane movement. *J. Atmos. Sci.*, **50**, 62-76.

_____, and _____, 1994: On hurricane outflow structure. *J. Atmos. Sci.*, **51**, 1995-2003.

_____, and _____, 1995a: Potential vorticity diagnostics of hurricane movement. Part I: A case study of Hurricane Bob (1991). *Mon. Wea. Rev.*, **123**, 69-92.

_____, and _____, 1995b: Potential vorticity diagnostics of hurricane movement. Part II: Tropical Storm Ana (1991) and Hurricane Andrew (1992). *Mon. Wea. Rev.*, **123**, 93-109.

_____, and Y. Kurihara, 1996: A numerical study of the feedback mechanisms of hurricane-environment interaction on hurricane movement from the potential vorticity perspective. *J. Atmos. Sci.*, **53**, 2264-2282.

TEST TARGET (QA-3)

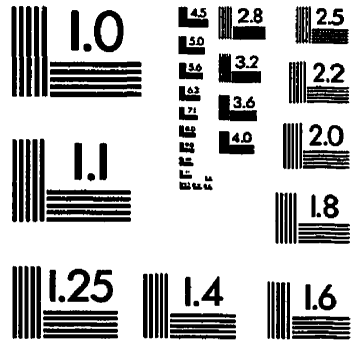

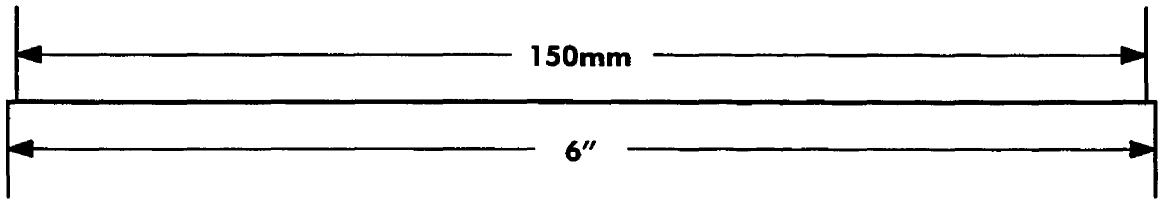

APPLIED IMAGE, Inc
1653 East Main Street
Rochester, NY 14609 USA
Phone: 716/482-0300
Fax: 716/288-5989